

Efficiency of black hole formation via collisions in stellar systems

Data analysis from simulations and observations

M.C. Vergara^{1*}, D.R.G. Schleicher^{2**}, A. Escala^{3***}, B. Reinoso⁴, F. Flammini Dotti¹, A. W. H. Kamlah^{1,5},
M. Liempi², N. Hoyer^{6,5}, N. Neumayer⁵, and R. Spurzem^{1,7,8}

- ¹ Astronomisches Rechen-Institut, Zentrum für Astronomie, University of Heidelberg, Mönchhofstrasse 12-14, 69120, Heidelberg, Germany
- ² Departamento de Astronomía, Facultad Ciencias Físicas y Matemáticas, Universidad de Concepcion, Av. Esteban Iturra s/n Barrio Universitario, Casilla 160-C, Concepcion, Chile
- ³ Departamento de Astronomía, Universidad de Chile, Casilla 36-D, Santiago, Chile
- ⁴ Universität Heidelberg, Zentrum für Astronomie, Institut für Theoretische Astrophysik, Albert-Ueberle-Str. 2, 69120 Heidelberg, Germany
- ⁵ Max-Planck-Institut für Astronomie, Königstuhl 17, 69117 Heidelberg, Germany
- ⁶ Donostia International Physics Center, Paseo Manuel de Lardizabal 4, E-20118 Donostia-San Sebastián, Spain
- ⁷ National Astronomical Observatories and Key Laboratory of Computational Astrophysics, Chinese Academy of Sciences, 20A Datun Rd., Chaoyang District, Beijing 100012, China
- ⁸ Kavli Institute for Astronomy and Astrophysics, Peking University, Yiheyuan Lu 5, Haidian Qu, 100871, Beijing, China

Received September 15, XXXX; accepted March 16, YYYY

ABSTRACT

Context. This paper explores the theoretical relation between star clusters and black holes within them, focusing on the potential role of nuclear star clusters (NSCs), globular clusters (GCs), and ultra-compact dwarf galaxies (UCDs) as environments that allow for black hole formation via stellar collisions.

Aims. This study aims to identify the optimal conditions for stellar collisions across a range of stellar systems, leading to the formation of very massive stars that subsequently collapse into black holes. We analyze data from numerical simulations and observations of diverse stellar systems, encompassing various initial conditions, initial mass functions, and evolution scenarios.

Methods. We computed a critical mass, determined by the interplay of the collision time, system age, and initial properties of the star cluster. The efficiency of black hole formation (ϵ_{BH}) is defined as the ratio of initial stellar mass divided by the critical mass.

Results. We find that stellar systems with a ratio of initial stellar mass over critical mass above 1 exhibit a high efficiency in terms of black hole formation, ranging from 30 – 100%. While there is some scatter, potentially attributed to complex system histories and the presence of gas, the results highlight the potential for achieving high efficiencies via a purely collisional channel in black hole formation.

Conclusions. In conclusion, this theoretical exploration elucidates the connection between star clusters and black hole formation. The study underscores the significance of UCDs, GCs, and NSCs as environments conducive to the black hole formation scenario via stellar collisions. The defined black hole formation efficiency (ϵ_{BH}) is shown to be influenced by the ratio of the initial stellar mass to the critical mass.

Key words. Methods: numerical, Galaxies: nuclei, Galaxies/quasars: supermassive black holes, Galaxies: star clusters: general

1. Introduction

The origin of one of the most compact massive objects in the Universe, namely, supermassive black holes (SMBHs) has not been determined thus far. These objects exhibit masses ranging between $10^6 - 10^{10} M_{\odot}$ (Natarajan & Treister 2009; Volonteri 2010; Kormendy et al. 2010; Kormendy & Ho 2013; McConnell et al. 2011; Zuo et al. 2015; King 2016; Pacucci et al. 2017; Mehrgan et al. 2019; Onken et al. 2020). Remarkable findings on SMBHs in the distant universe have been published by different research teams, starting from the first three quasars observed

at redshift (z) higher than 6 reported by Fan et al. (2003). Afterward, Mortlock et al. (2011) observed a quasar at $z = 7.085$ with a mass of $2 \times 10^9 M_{\odot}$. Soon after, Wu et al. (2015) discovered one of the most massive SMBHs known to date, weighing in at $1.2 \times 10^{10} M_{\odot}$ at $z = 6.3$. A few years later, Jeram et al. (2020) found a quasar at $z = 2.89$ with a mass of $2.7 \times 10^{10} M_{\odot}$, which is believed to be the most massive SMBH known thus far. Additionally, Wang et al. (2021) contributed to the exploration by spotting a distant active galactic nucleus (AGN) at $z = 7.642$, with a mass of $(1.6 \pm 0.4) \times 10^9 M_{\odot}$. Bañados et al. (2016) provided the observation of more than 100 quasars with redshifts between $5.6 \lesssim z \lesssim 6.7$. Most recently, Fan et al. (2023) presented a review of high redshift quasars that includes more than 300 quasars at $z > 6$.

* E-mail: Marcelo.C.Vergara@uni-heidelberg.de (MV)

** E-mail: dschleicher@astro-udec.cl (DS)

*** E-mail: aescala@das.uchile.cl (AE)

Some scenarios depict SMBH formation as being related to the remnants of population III stars (Machida & Doi 2013; Latif et al. 2014; Riaz et al. 2022). These stars usually form in metal-free clouds and accumulate mass onto their cores (Omukai & Nishi 1998; Volonteri et al. 2003; Tan & McKee 2004; Ricarte & Natarajan 2018). Another possible route is the direct collapse model, where massive gas clouds collapse within atomic cooling halos at high redshift (Bromm & Loeb 2003; Volonteri et al. 2008; Latif et al. 2013; Latif & Schleicher 2015; Zwick et al. 2023) and runaway collisions and mergers of stars take place within star clusters (Rees 1984; Portegies Zwart & McMillan 2002; Fujii & Portegies Zwart 2013; Katz et al. 2015; Sakurai et al. 2017; Reinoso et al. 2018, 2020; Sakurai et al. 2019; Vergara et al. 2021, 2023). In addition, some authors have proposed runaway collisions and mergers with gas accretion to explain their origins (Boekholt et al. 2018; Regan et al. 2020; Chon & Omukai 2020; Das et al. 2021; Schleicher et al. 2022, 2023; Reinoso et al. 2023). Runaway stellar collisions can lead to the formation of a very massive star (VMS), which eventually results in a supernova and/or forms a stellar mass black hole (Heger & Woosley 2002; Whalen et al. 2013; Chen et al. 2014). The interaction of the black hole with stars or other stellar mass black holes, besides their capacity to accrete surrounding material, can lead to the formation of an intermediate-mass black hole (IMBH) (Arca Sedda et al. 2023a,b,c). Stellar systems where this process may potentially occur include NSCs (Georgiev et al. 2016; Neumayer et al. 2020), GCs (Lützgendorf et al. 2011, 2012, 2013b), and UCDs (Seth et al. 2014; Ahn et al. 2017, 2018; Voggel et al. 2018). Regardless of their different ages, sizes, and masses (i.e., density), all of them offer suitable environments for stellar dynamics to unfold.

As one of the densest stellar configurations known in the Universe, NSCs usually fall in the mass range of $10^5 - 10^7 M_{\odot}$ (Böker et al. 2002; Walcher et al. 2005; Côté et al. 2006; Böker 2010; Georgiev et al. 2009, 2016; Fritz et al. 2016; Ordenes-Briceño et al. 2018; Sánchez-Janssen et al. 2019; Neumayer et al. 2020), with a half-mass radius of a few parsecs to a few tens of parsecs (Georgiev et al. 2016). Typically, NSCs contain multiple stellar populations, since they can host old stars, however, they also present star formation (Walcher et al. 2005; Rossa et al. 2006; Kacharov et al. 2018). Also, they can coexist with SMBHs (Neumayer & Walcher 2012; Georgiev et al. 2016; Neumayer et al. 2020; Escala 2021; Vergara et al. 2023). There are correlations of the SMBH mass with the mass of the galactic bulge (Magorrian et al. 1998; Marconi & Hunt 2003; Häring & Rix 2004), the SMBH mass and the velocity dispersion of the surrounding stars (Ferrarese & Merritt 2000; Tremaine et al. 2002; Gültekin et al. 2009), as well as between the luminosity of the galaxy bulge and the NSC mass (Ferrarese et al. 2006; Rossa et al. 2006; Wehner & Harris 2006; Böker 2008; Savorgnan et al. 2016). Investigations of stellar orbits surrounding the SMBH at the center of the Milky Way (Ghez et al. 2008; Genzel et al. 2010; Gillessen et al. 2017), as well as the observation of the shadow of Sagittarius A* (Event Horizon Telescope Collaboration et al. 2022) provide evidence that there is a central massive object (Genzel et al. 2010; Schödel et al. 2014). The simultaneous presence of SMBHs and NSCs occur in galaxies with masses around $\sim 10^{10} M_{\odot}$ (Seth et al. 2008). In less massive galaxies, which have less massive SMBHs, direct observations of their dynamical imprint on the NSCs are a challenging task that requires higher spatial resolution than for more massive galaxies at the same distance. Some studies have proposed the absence of a black hole or have set an upper limit on its mass with $M_{\text{BH}} < 1500 - 3000 M_{\odot}$ (Gebhardt et al. 2001; Merritt

et al. 2001). Other examples of NSCs with upper limits for black holes are NGC 300 and NGC 428 (Neumayer & Walcher 2012). The gravitational influence of the Galactic center has a strong effect on the surrounding gas and stars, causing them to fall to the Galactic center by gradually losing their angular momentum (Shlosman et al. 1990; Escala 2006). At high redshifts, the absence of SMBHs at Galactic centers and the abundance of gas lead to even stronger inflows, resulting in the formation of highly dense regions composed of stars and gas (Prieto & Escala 2016). Other proposed accretion mechanisms include clump migration through dynamical friction (Tremaine et al. 1975; Escala 2007; Elmegreen et al. 2008; Arca-Sedda & Capuzzo-Dolcetta 2014; Aharon & Perets 2015) and gravitational torques during galaxy mergers (Barnes & Hernquist 1991; Barnes 2002; Mayer et al. 2010; Newton & Kay 2013; Wurster & Thacker 2013; Blumenthal & Barnes 2018; Prieto et al. 2021).

With a half-mass radius of approximately $\sim 10 - 50$ pc (Seth et al. 2014; Ahn et al. 2018; Faifer et al. 2017) and masses of $10^6 - 10^8 M_{\odot}$ (Dabringhausen et al. 2009, 2010), UCDs stand as the densest stellar systems of the Universe. They are known to be old systems, but determining their age and metallicity can be challenging (Chilingarian & Mamon 2008; Francis et al. 2012). Their origins are still unclear, with some theories proposing them to be massive star clusters formed through the merger of smaller GCs (Kroupa 1998; Fellhauer & Kroupa 2002; Fellhauer et al. 2002; Urrutia Zapata et al. 2019) or remnants of tidally stripped dwarf galaxies (Bassino et al. 1994; Bekki & Freeman 2003; Pfeffer & Baumgardt 2013). Examples of these objects include UCD 330, UCD 320 (Voggel et al. 2018), M60-UCD1 (Seth et al. 2014), M59c0 (Ahn et al. 2017), M59-UCD-3 (Ahn et al. 2018), and FUCD3 (Afanasyev et al. 2018).

Stellar systems with a lower central density compared to NSCs are known as GCs, with half-mass radii of a few to several dozen parsecs and masses of $10^4 - 10^6 M_{\odot}$. These clusters are predominantly populated by primordial stars, indicating ages of over 10 billion years (Kravtsov & Gnedin 2005). They are found in the halos of galaxies, typically at distances of tens of thousands of light years from the Galactic center. Most of the GCs in the Milky Way originate from a dual process: star formation during the early stages of cosmic evolution and the gradual disruption of dwarf galaxies (White & Rees 1978; Kruijssen et al. 2019). Some examples of GCs are ω Cen, 47Tuc, M15, or M80 (Harris 1996). These stellar systems (NSCs, UCDs, and GCs) provide an ideal environment for stellar collisions to occur.

In general, clusters with a total mass below $10^5 M_{\odot}$ are not very dense, but can form black holes of a relatively low mass, typically amounting to a few percent of the initial mass (Portegies Zwart et al. 1999; Fujii & Portegies Zwart 2013; Koliopanos 2017; Arca Sedda et al. 2023a,b,c). Simulations of more massive clusters ($< 10^7 M_{\odot}$) are computationally expensive. However, by adopting approximations, they can be explored via Fokker-Planck models at higher cluster masses (Lee 1987; Quinlan & Shapiro 1990; Stone et al. 2017). Escala (2021) proposed that the formation of massive objects in dense stellar systems is regulated by the relation between the collision time in a given system with the age and the relaxation time of that system, as it determines both whether collisions may efficiently occur and whether the system as a whole will be able to readjust to possible changes as a result of collisions. Vergara et al. (2023) performed N-body simulations to probe this scenario further. From the comparison of the collision time with the age of the system, they derived a critical mass, M_{crit} , which is the mass at which the collision timescale becomes equal to the age of the system. This implies that the large majority of stars in the system could then be ex-

pected to go through a collision, implying a drastic growth of the most massive objects. Indeed, Vergara et al. (2023) found that the mass of the most massive object systematically increases with the ratio of the initial mass divided by the critical mass (M_i/M_{crit}). In addition, a very similar relation has been found in a preliminary comparison with observed NSCs (Escala 2021).

In this paper, we aim for a more systematic investigation of the same relation reported in Vergara et al. (2023). We present and compare a range of simulation results from different investigations in terms of M_i/M_{crit} values and the growth of the most massive object. In particular, the set of simulations analyzed here includes different radial profiles and initial mass functions, as well as models for stellar evolution; for instance, employing realistic simulations of GCs, such as DRAGON II (Arca Sedda et al. 2023a,b,c). We also aim to further refine the comparison with observational data, including additional NSCs, improved age estimates, and additional stellar systems such as GCs and UCDs.

The paper is organised as follows. Section 2 summarizes the methodology and data employed. Section 3 shows the results of our analysis. Section 4 provides a summary of conclusions drawn from our investigation.

2. Methodology

Here, we employed and tested the concept of the critical mass (M_{crit}) introduced by Vergara et al. (2023), which is described in Section 2.1. We accounted for the potential presence of an external potential, namely, one that is due to the presence of gas in the stellar system. To test this concept, we gathered data from multiple sources of N-body simulations, from which we determined both M_{crit} and the black hole formation efficiency (ϵ_{BH}), which is presented in Section 2.2. These were computed using various initial conditions such as the initial stellar system mass, M_i , number of stars, N , the half-mass radius, R_h , the stellar mass, m_* , and radius, r_* , besides the mass of the most massive object, M_{BH} , and age, τ , at the end of the simulations. A summary of the parameter space explored by different authors is provided in our Table 1 for simulations without any external potential and in Table 2 for simulations with external potential. We further employed observations of NSCs, GCs, and UCDs (Table 3, 4, and 5, respectively). From these data, we use the current age, τ ; mass, M_i ; and effective radius, R_{eff} , of the stellar system, besides the mass of the black hole, M_{BH} .

2.1. Critical mass

The critical mass, introduced in Vergara et al. (2023) is:

$$M_{\text{crit}} = R_h^{7/3} \left(\frac{4\pi m_*}{3\Sigma_0 \tau G^{1/2}} \right)^{2/3}, \quad (1)$$

where R_h is the half-mass radius of the stellar system, m_* is the average mass of a star within the cluster, τ is the age of the system, G is the gravitational constant, $\Sigma_0 = 16\sqrt{\pi}r_*^2(1 + \Theta)$ is the cross-section for collisions (including gravitational focusing), and $\Theta = 9.54(m_*R_\odot/r_*M_\odot)(100 \text{ km s}^{-1}/\sigma)^2$ is the Safronov number (where r_* is the stellar radius and σ the velocity dispersion of the stellar system). We evaluated the Safronov number assuming virial equilibrium ($\sigma = \sqrt{GM/R}$), which is commonly employed in the initial conditions of numerical simulations.

In the presence of an external potential due to the presence of gas with a mass, M_g , within the stellar system, it is straightforward to generalize this expression under the assumption of virialization with the formalism employed by Reinoso et al. (2020), namely,

$$M_{\text{crit,ext}} = R_h^{7/3} \left(\frac{4\pi m_*}{3\Sigma_0 \tau G^{1/2}} \right)^{2/3} (1+q)^{-2/3}, \quad (2)$$

with $q = M_g/M_i$. The presence of the external potential thus effectively reduces the critical mass, as it increases the velocity dispersion in the stellar system and therefore increases the likelihood for collisions to occur during the age of the system.

2.2. Black hole formation efficiency

The other central quantity in this paper is the black hole formation efficiency (ϵ_{BH}), which is defined as the mass of the most massive object formed via collisions divided by the final stellar mass of the stellar system:

$$\epsilon_{\text{BH}} = (1 + M_f/M_{\text{BH}})^{-1}. \quad (3)$$

We note, in particular, that the gas mass is not being considered in the definition of ϵ_{BH} , especially as we are not considering the effects of accretion, whereas the possible effects of the gas are only included through its effect on the steepening of the gravitational potential. A more detailed treatment of the gas would lead to accretion and would make the system more dissipative overall, thereby increasing the masses of the most massive objects to form. However, such a treatment is beyond the scope of the present paper.

2.3. Numeric models

In this subsection, we compile the data from different sources of N-body simulations. These simulations were performed using different codes, including BRIDGE (Fujii et al. 2007), STARLAB (McMillan 1996), NBODY6 (Aarseth 1999b,a), NBODY6++GPU (Wang et al. 2015), and BIFROST (Rantala et al. 2023). These codes have included different models for the star distribution, including profiles corresponding to Plummer (1911); King (1966); Miyamoto & Nagai (1975). They also employ different assumptions concerning the stellar mass function, including models with equal mass stars or employing an initial mass function (IMF) (Salpeter 1955; Scalo 1986; Kroupa 2001). In the following, we briefly describe the different simulations considered in this investigation.

Fujii & Portegies Zwart (2013) explored the role of stellar collisions in virialized isolated cluster models, using a Salpeter (1955) IMF and the King (1966) density profile. While Sakurai et al. (2017) explored runaway collisions in first star clusters, using the IMF from Salpeter (1955). The distribution of stars was obtained from cosmological hydrodynamical simulations. Both studies use the BRIDGE code (Fujii et al. 2007)

Portegies Zwart et al. (1999) investigated runaway collisions in young compact star clusters, utilizing a Scalo (1986) IMF, while Mapelli (2016) explored the impact of metallicity on runaway collisions, employing a Kroupa (2001) IMF. Both investigations employed a King (1966) profile and the STARLAB software (McMillan 1996).

Katz et al. (2015) investigated collisions in primordial star clusters at high redshift, using a Salpeter (1955) IMF. Reinoso et al. (2018) studied collisions in primordial star clusters, employing equal-mass stars. Reinoso et al. (2020) explored runaway collisions in dense star clusters, considering the effects of an external potential. Katz et al. (2015); Reinoso et al. (2018, 2020) used Plummer models (Plummer 1911). Vergara et al.

(2021) investigated collisions in flat and rotating clusters using a Miyamoto-Nagai distribution (Miyamoto & Nagai 1975). All studies used the NBODY6 code (Aarseth 2000).

Panamarev et al. (2019) simulated the Galactic center of the Milky Way using one million particles, despite the galactic center having approximately more stars by two orders of magnitude, the computational limitations prevent the inclusion of a higher number of stars, the study employed the IMF from Kroupa (2001). Vergara et al. (2023) explored runaway collisions in NSCs, using models with equal-mass stars. Arca Sedda et al. (2023a,b,c), investigated star cluster evolution with up to one million stars, these are some of the most realistic simulations (DRAGON-II), including a Kroupa (2001) IMF, primordial binaries, stellar evolution, and dynamics of compact objects. All studies use a Plummer distribution (Plummer 1911). The simulations employed the NBODY6++GPU code (Wang et al. 2015). Rizzuto et al. (2023) simulated dense clusters of low mass stars, using a Kroupa (2001) IMF and including an initial central black hole. This work was made with the BIFROST code (Rantala et al. 2023).

The key parameters for computing the critical mass and black hole formation efficiency are summarized in Table 1. In addition, in Table 2, we show the simulations of Reinoso et al. (2020), where we include $q = M_g/M_i$. The complete Tables 1 and 2 are available online (see Appendix A for more details).

The DRAGON simulations (Wang et al. 2016) are excluded from this analysis. Although these simulations give rise to multiple black holes, none of the simulations exhibit a dominant mass and therefore do not become the most massive object in the cluster.

All the previously mentioned simulations employ N-body codes to study the stellar dynamics. While they share some similarities, they also have differences. The principal algorithm shared between codes is the Hermite integrator scheme, while BRIDGE uses a sixth-order scheme. The other three codes use a fourth-order scheme. Moreover, NBODY6 and NBODY6++GPU are direct N-body codes and have several algorithms in common, such as the Kustaanheimo-Stiefel regularization to solve close encounters (Stiefel & Kustaanheimo 1965), chain regularization (Mikkola & Aarseth 1990, 1993), and the Ahmad-Cohen neighbor scheme which spatially splits the hierarchy of the stars to speed up computational calculations (Ahmad & Cohen 1973). Indeed, NBODY6++GPU is the improved version of NBODY6, thus NBODY6++GPU is optimized with GPU-accelerated supercomputing, which speeds up the calculations. This code also incorporates algorithms for solving stellar dynamics and recipes for stellar evolution proposed by Hurley et al. (2000, 2002), implemented by Kamlah et al. (2022). On the other hand, the most recent version of STARLAB is also a direct N-body code, adopted the stellar evolution recipe by Hurley et al. (2000); however, in the past, the code used recipes from Portegies Zwart & Verbunt (1996) for stellar evolution, incorporating the Eggleton & Tout (1989) mass-loss equations and the Schaerer (1999) model for massive stars losing their hydrogen envelope. BRIDGE is a tree-direct hybrid N-body code. The internal region of the cluster is accurately solved through direct integration using the Hermite scheme (Nitadori & Makino 2008), while the external motion is computed employing the tree algorithm (Barnes & Hut 1986; Makino 2004). The separation between the tree and direct calculations is achieved through Hamiltonian splitting (Kinoshita et al. 1990; Wisdom & Holman 1991). Finally, BIFROST is a direct summation N-body code accelerated by GPU with a hierarchical formulation of fourth-order forward symplectic integrator, originating in FROST (Rantala et al. 2021), the precursor of BIFROST,

Table 1. Initial conditions for simulation sets

M_i [M_\odot]	R_h [pc]	N	M_{BH} [M_\odot]	τ [Myr]	Code	Ref.
8233	0.25	12288	140	5.5	SL	P+99
8233	0.25	12288	100	4.5		
...		
6300	0.10	2048	182	5	B	F+13
25000	0.22	8192	399	5		
...		
10100	0.06	14429	694.5	3.5	NB6	K+15
10100	0.11	14429	494	3.5		
...		
65000	0.98	100000	22	17	SL	M+16
65000	0.98	100000	212	17		
...		
164000	1.07	19900	929	3	B	S+17
130000	0.84	15700	409	3		
...		
10000	0.10	100	300	2	NB6	R+18
10000	0.10	100	300	2		
...		
618000	4.20	1000000	10000	5500	NB6+	P+19
10000	0.11	100	350	15.6	NB6	R+20
10000	0.11	100	466	15.6		
...		
100000	0.08	1000	6310	2	NB6	V+21
100000	0.08	10000	39800	2		
...		
50000	0.008	1000	9917	10	NB6+	V+23
25000	0.008	500	3850	10		
...		
70000	1.75	120000	64	2379	NB6+	AS+23
180000	1.75	300000	69	1196		
...		
89590	0.4	256000	1152	41.2	BF	R+23
89590	0.6	256000	1329	148		
...		

Notes. Summary of the initial conditions for the different sets of simulations. The first and second columns are M_i and R_h which are the initial mass and half-mass radius of the stellar system, respectively. The third column is the number of stars. The fourth column M_{BH} is the black hole mass. The fifth is the time of the simulation. The sixth column shows the codes (B: bridge, SL: starlab, NB6: nbody6, NB6+: nbody6++gpu, and BF: bifrost) and the last column shows the references. The full table is available at the CDS.

References. P+99: Portegies Zwart et al. (1999), F+13: Fujii & Portegies Zwart (2013), K+15: Katz et al. (2015), M+16: Mapelli (2016), S+17: Sakurai et al. (2017), R+18: Reinoso et al. (2018), P+19: Panamarev et al. (2019), R+20: Reinoso et al. (2020), V+21: Vergara et al. (2021), V+23: Vergara et al. (2023), AS+23: Arca Sedda et al. (2023a,b,c), R+23: Rizzuto et al. (2023).

where the integrator was initially derived and tested. We note that the code PETAR (Wang et al. 2020) has been used to study mergers in star clusters (Wang et al. 2024; Barber et al. 2024) and population III star clusters (Wang et al. 2022; Liu et al. 2023). Although we did not include this data, Wang et al. (2022) simulations fall within $M_i/M_{crit} < 0.001$, keeping our conclusions unchanged. More information about algorithms of stellar dynamics is available in the review of computational methods for collisional stellar systems made by Spurzem & Kamlah (2023).

Table 2. Initial conditions for simulation sets with external potential

M_i [M_\odot]	R_h [pc]	N	M_{BH} [M_\odot]	τ [Myr]	q	Code	Ref.
10000	0.11	100	683	16.5	1.0	NB6	R+20*
10000	0.11	100	983	16.5	1.0		
...		

Notes. Summary of the initial conditions for the different sets of simulations with external potential. Same columns as in Table 1, adding an extra column q . The full table is available at the CDS.

References. R+20*: [Reinoso et al. \(2020\)](#)

2.4. Observations

In this subsection, we summarize the observational data on different types of stellar systems we employ in this analysis, considering NSCs, UCDs, and GCs. We summarize the critical parameters, including the age of the cluster, the effective radii, the masses of the stars, and the black hole within in Table 3 (NSCs), Table 4 (GCs), and Table 5 (UCDs). We note that for all stellar systems, we assumed that the initial mass is the sum of the current stellar mass and the mass of the black hole¹.

We assumed that the initial mass of the galactic center was the combined mass of the black hole and NSC ([Vergara et al. 2023](#)). Additionally, we considered the initial effective radius to be one-tenth of its current size, as suggested by [Banerjee & Kroupa \(2017\)](#). We assumed that the stars have solar properties (i.e., $1 M_\odot$ and $1 R_\odot$). If the NSCs ages were not available we assume a typical age of 8 Gyr.

For the GCs, we made the same assumption for the initial mass as for NSC (i.e., $M_i = M_{\text{GC}} + M_{\text{BH}}$). These stellar configurations are one of the oldest objects in the Universe. The effective radius of isolated GCs remains constant through several relaxation timescales ([Spitzer & Thuan 1972](#)), then we assume that the current size mirrors the initial size. GCs are old stellar systems. If the age was not available, we assumed a typical age of 12 Gyr.

We analyzed the UCDs by taking into account assumptions from both GCs and NSCs regarding their effective radius; for the initial mass, we consider $M_i = M_{\text{UCD}} + M_{\text{BH}}$, given the uncertain nature of their formation. Some theories propose that UCDs could be remnants of tidal disruptions in dwarf galaxies interacting with larger ones, resulting in the stripping of outer layers and the formation of NSCs ([Bassino et al. 1994](#); [Bekki & Freeman 2003](#); [Pfeffer & Baumgardt 2013](#)). Alternatively, there is a suggestion that UCDs may originate from the merger of multiple GCs ([Kroupa 1998](#); [Fellhauer & Kroupa 2002](#); [Fellhauer et al. 2002](#); [Urrutia Zapata et al. 2019](#)). In our investigation of UCDs, we considered two scenarios. In particular, UCD1 assumes a fixed radius during evolution, incorporating an external potential with 80% dark matter due to observed high mass-to-light ratio values ([Baumgardt & Mieske 2008](#)); UCD2, aligning more with [Fellhauer & Kroupa \(2006\)](#), posits an absence of dark matter and envisions an initial expansion like NSCs. Determining the ages of UCDs is a challenging task ([Francis et al. 2012](#)).

¹ In principle, additional mass loss could have occurred, as we also find in our simulations. We checked that very similar results are obtained if we apply the same correction factor (accounting for mass loss) as we did in the case of simulations. However, in real physical systems, the situation may be more complex; particularly in the case of NSCs, they could also gain mass both due to in situ star formation and mergers with GCs. We therefore prefer to stick with a minimal set of assumptions within the analysis.

For those stellar systems that do not present an age measurement, we assumed a typical age in between GCs and NSCs of 10 Gyr.

3. Data analysis and comparison

In this section, we use the available data on simulations and observations to systematically test the concept of the critical mass. For this purpose, we first briefly recall the main differences between the respective datasets. In the case of simulations, we recall they represent idealized isolated systems. In most cases in the literature, their initial conditions, including the initial stellar mass, M_i , have been reported, as well as the main outcomes, such as the mass M_{BH} of the massive object that forms. In the case of observational data, on the other hand, we know about the current state of the system, namely, the final stellar mass, M_f , and the mass of the most massive object, M_{BH} . We also note that real observational systems may be more complex than the simulation and may include additional physical processes. In the case of NSCs, gas physics, star formation, and mergers with GCs could play some role in their evolution. For GCs and UCDs, on the other hand, it is more plausible that the stellar systems might be evolving for very long timescales essentially in isolation and without active star formation.

The computation of the critical mass (as defined via Eq. 2) does, in principle, require knowledge of the initial conditions and is relatively trivial in the case of numerical simulations, while in the case of observations some assumptions or estimates may be necessary to determine the critical mass scale. On the other hand, the efficiency parameter ϵ_{BH} defined in Eq. 3 requires knowledge of the final stellar mass and the mass of the most massive object. This appears straightforward from an observational perspective, whereas in simulations, the final stellar mass has not always been documented and may thus require an estimate. In the following subsections, we first analyse the results from simulations and observations separately and subsequently attempt to make a comparison between simulation and observation results.

3.1. Simulations data

In simulations, the initial conditions are known, and the calculation of the critical mass, M_{crit} , and the ratio, M_i/M_{crit} , is thus straightforward. Information about the final stellar mass is, in principle, part of the simulations, but has not usually been reported in the literature. A first simple estimate can be obtained if the mass loss is neglected, but still considering the mass that has gone into the most massive object, implying:

$$M_f = M_i - M_{\text{BH}}. \quad (4)$$

The result of this calculation is given in the left panel of Fig. 1. While we found scatter in the plot, we can clearly note that higher efficiencies, ϵ_{BH} , are obtained in all simulations with $M_i/M_{\text{crit}} \gtrsim 0.3$ with an increasing trend, the slope of this trend depending somewhat on the set of simulations being considered, with maximum efficiencies reaching around 40 – 50%. On the other hand, for low values of M_i/M_{crit} , the relation appears essentially flat with efficiencies (at best) on the level of a few percent.

In the left panel of Fig. 1, mass loss via escapers has been completely neglected, while (in principle) it is clear that it should be considered. We know however at least from some simulations how much mass has been lost during evolution. In Appendix B, we employ the simulations of [Vergara et al. \(2021, 2023\)](#); [Reinoso et al. \(2020\)](#) to analyze how the ratio M_f/M_i depends on M_i/M_{crit} . Such a dependence can be expected for two

Table 3. Observational properties of NSCs.

ID	$M_{\text{BH}} [M_{\odot}]$	Ref.	$M_{\text{NSC}} [M_{\odot}]$	Ref.	$R_{\text{eff}} [\text{pc}]$	Ref.	$\tau [\text{Myr}]$	Ref.
MW	4.04×10^6	(1, 2)	2.50×10^7	(3)	4.20	(3)	5.5×10^3	(4, 5)
IC342	3.16×10^5	(6)	1.25×10^7	(6)	1.39	(6)	3.4×10^1	(6)
NGC205	6.80×10^3	(8)	2.50×10^6	(7)	1.30	(7)	3.0×10^3	(9, 10)
NGC221	2.50×10^6	(7)	1.70×10^7	(7)	4.40	(7)	2.9×10^3	(11)
NGC404	5.50×10^5	(12)	1.10×10^7	(13)	15.00	(13)	1.0×10^3	(13)
NGC428	3.00×10^4	(14)	2.60×10^6	(14)	1.20	(15)	1.8×10^3	(16)
NGC1042	2.50×10^4	(14)	3.20×10^6	(14)	1.30	(15)	1.1×10^4	(16)
NGC1336	4.30×10^7	(17)	7.00×10^8	(18)	66.50	(19)	8.0×10^3	(18)
NGC1493	2.50×10^5	(14)	3.50×10^6	(14)	3.60	(15)	5.7×10^3	(16)
NGC2139	1.50×10^5	(14)	2.70×10^7	(15)	14.80	(15)	4.1×10^1	(16)
NGC2787	4.10×10^7	(20)	7.00×10^7	(21)	5.10	(22)	8.0×10^3	(*)
NGC3115	9.10×10^8	(23)	7.20×10^6	(24)	6.60	(22)	5.0×10^3	(25)
NGC3368	7.50×10^6	(26)	4.80×10^7	(27)	10.40	(27)	3.0×10^3	(28)
NGC3423	1.50×10^5	(14)	1.90×10^6	(15)	2.20	(15)	5.6×10^3	(16)
NGC3593	2.40×10^6	(29)	1.70×10^7	(29)	5.10	(22, 29)	2.0×10^3	(30)
NGC3621	3.00×10^6	(31)	6.50×10^6	(15)	1.80	(15)	1.6×10^3	(32)
NGC4395	3.60×10^5	(33, 34)	2.00×10^6	(15, 33)	1.50	(15)	3.0×10^3	(33)
NGC4414	1.50×10^6	(35)	1.20×10^8	(15)	26.50	(15)	4.5×10^3	(35)
NGC4486	6.60×10^9	(36)	2.00×10^8	(14)	7.40	(37)	8.0×10^3	(*)
NGC4501	1.90×10^7	(26)	5.20×10^8	(27)	30.00	(27)	7.5×10^3	(38)
NGC4578	3.50×10^7	(39)	5.30×10^7	(40)	7.03	(40)	8.0×10^3	(*)
NGC4623	1.60×10^8	(41)	1.30×10^8	(40)	48.03	(40)	8.0×10^3	(*)
NGC4697	1.70×10^8	(42)	2.80×10^7	(24)	4.40	(24)	8.9×10^3	(43)
NGC4699	1.54×10^{10}	(26)	6.30×10^8	(27)	25.75	(27)	8.0×10^3	(*)
NGC5055	8.50×10^8	(20)	1.70×10^6	(22)	13.50	(22)	3.8×10^3	(28)
NGC5102	9.10×10^5	(8)	7.30×10^7	(7)	26.30	(7)	6.9×10^2	(32)
NGC5206	6.30×10^5	(8)	1.50×10^7	(7)	8.10	(7)	2.9×10^3	(32)
NGC7424	1.50×10^5	(14)	1.00×10^6	(14, 15)	6.80	(14, 15)	1.3×10^3	(16)
NGC7713	7.50×10^6	(44)	4.04×10^5	(22)	1.14	(22)	8.0×10^3	(*)
VCC1254	9.00×10^6	(45)	1.10×10^7	(24)	49.20	(24)	5.7×10^3	(46)

Notes. The columns are: (1) stellar system ID; (2, 3) BHs mass and reference; (4, 5) NSCs mass and reference; (6, 7) NSCs effective radius and reference; and (8, 9) age and reference. Note: for stellar systems where the age is not defined, we assumed a typical age, denoted by (*).

References. (1) GRAVITY Collaboration et al. (2018), (2) Do et al. (2019), (3) Schödel et al. (2014), (4) Blum et al. (1996), (5) Pfuhl et al. (2011), (6) Böker et al. (1999), (7) Nguyen et al. (2018), (8) Nguyen et al. (2019), (9) Cappellari et al. (1999), (10) Davidge (2003), (11) Villaume et al. (2017), (12) Davis et al. (2020), (13) Nguyen et al. (2017), (14) Neumayer & Walcher (2012), (15) Georgiev et al. (2016), (16) Walcher et al. (2006), (17) Thater et al. (2023), (18) Fahrion et al. (2019), (19) Turner et al. (2012), (20) Graham (2008), (21) Sarzi et al. (2001), (22) Pechetti et al. (2020), (23) Emsellem et al. (1999), (24) Graham & Spitler (2009), (25) Shcherbakov et al. (2014), (26) Saglia et al. (2016), (27) Ashok et al. (2023), (28) Sarzi et al. (2005), (29) Nguyen et al. (2022), (30) Coccato et al. (2013), (31) Barth et al. (2009), (32) Kacharov et al. (2018), (33) den Brok et al. (2015), (34) Peterson et al. (2005), (35) Thater et al. (2017), (36) Gebhardt et al. (2011), (37) Gnedin et al. (2014), (38) Repetto et al. (2017), (39) Krajnović et al. (2018), (40) Côté et al. (2006), (41) Pechetti et al. (2017), (42) Gebhardt et al. (2003), (43) Trager et al. (2000), (44) Fusco et al. (2022), (45) Geha et al. (2002) (46) Paudel et al. (2011).

Table 4. Observational properties of GCs.

ID	$M_{\text{BH}} [M_{\odot}]$	Ref.	$M_{\text{GC}} [M_{\odot}]$	Ref.	$R_{\text{eff}} [\text{pc}]$	Ref.	$\tau [\text{Myr}]$	Ref.
G1	2.30×10^4	(1)	5.75×10^6	(2)	6.50	(3)	13.0×10^3	(13)
NGC104	1.50×10^3	(4)	1.10×10^6	(1)	4.10	(5)	10.7×10^3	(14)
NGC1851	2.00×10^3	(6)	3.72×10^5	(6)	1.80	(5)	8.8×10^3	(14)
NGC1904	3.00×10^3	(6)	1.41×10^5	(6)	2.40	(5)	9.4×10^3	(14)
NGC2808	1.00×10^4	(7)	8.13×10^5	(7)	2.20	(5)	8.2×10^3	(14)
NGC5139	4.70×10^4	(8)	2.51×10^6	(8)	7.60	(5)	12.0×10^3	(*)
NGC5286	1.50×10^3	(9)	2.82×10^5	(9)	2.50	(5)	12.0×10^3	(*)
NGC5694	8.00×10^3	(6)	2.57×10^5	(6)	4.10	(5)	11.4×10^3	(14)
NGC5824	6.00×10^3	(6)	4.47×10^5	(6)	4.20	(5)	10.9×10^3	(14)
NGC6093	8.00×10^2	(6)	3.39×10^5	(6)	1.80	(5)	13.0×10^3	(15)
NGC6266	2.00×10^3	(6)	9.33×10^5	(6)	1.80	(5)	10.0×10^3	(14)
NGC6388	1.70×10^4	(10)	1.10×10^6	(10)	1.50	(5)	12.0×10^3	(*)
NGC6715	9.40×10^3	(11)	1.91×10^6	(1)	6.30	(5)	12.0×10^3	(*)
NGC7078	4.40×10^3	(12)	6.17×10^5	(12)	3.00	(5)	10.3×10^3	(14)

Notes. The columns are the same as in Table 3.

References. (1) McLaughlin et al. (2006), (2) Gebhardt et al. (2005), (3) Ma et al. (2007), (4) Lützgendorf et al. (2013c), (5) Harris (1996), (6) Lützgendorf et al. (2013a), (7) Lützgendorf et al. (2012), (8) Noyola & Baumgardt (2011), (9) Feldmeier et al. (2013), (10) Lützgendorf et al. (2011), (11) Ibata et al. (2009), (12) Gerssen et al. (2002), (13) Meylan et al. (2001), (14) De Angeli et al. (2005), (15) Rosenberg et al. (1999).

Table 5. Observational properties of UCDs.

ID	$M_{\text{BH}} [M_{\odot}]$	Ref.	$M_{\text{UCD}} [M_{\odot}]$	Ref.	$R_{\text{eff}} [\text{pc}]$	Ref.	$\tau [\text{Myr}]$	Ref.
B023-G078	9.10×10^4	(1)	6.22×10^6	(1)	18.70	(1)	10.5×10^3	(1)
FUCD3	3.30×10^6	(2)	8.30×10^7	(2)	19.40	(2)	13.9×10^3	(10)
M59c0	5.80×10^6	(3)	8.30×10^7	(3)	32.00	(3)	9.3×10^3	(9)
M59-UCD-3	4.20×10^6	(4)	1.90×10^8	(4)	27.00	(4)	7.7×10^3	(7)
M60-UCD1	2.10×10^7	(5)	1.20×10^8	(5)	47.90	(5)	10.0×10^3	(*)
UCD330	1.00×10^5	(6)	6.10×10^6	(6)	3.11	(6)	10.0×10^3	(*)
UCD320	1.00×10^6	(6)	2.81×10^6	(6)	4.67	(6)	10.0×10^3	(*)
VUCD3	4.40×10^6	(3)	6.60×10^7	(3)	18.00	(3)	13.0×10^3	(8)

Notes. The columns are the same as in Table 3.

References. (1) Pechetti et al. (2022), (2) Afanasiev et al. (2018), (3) Ahn et al. (2017), (4) Ahn et al. (2018), (5) Seth et al. (2014), (6) Voggel et al. (2018), (7) Villaume et al. (2017), (8) Francis et al. (2012), (9) Chilingarian & Mamon (2008), (10) Chilingarian et al. (2011).

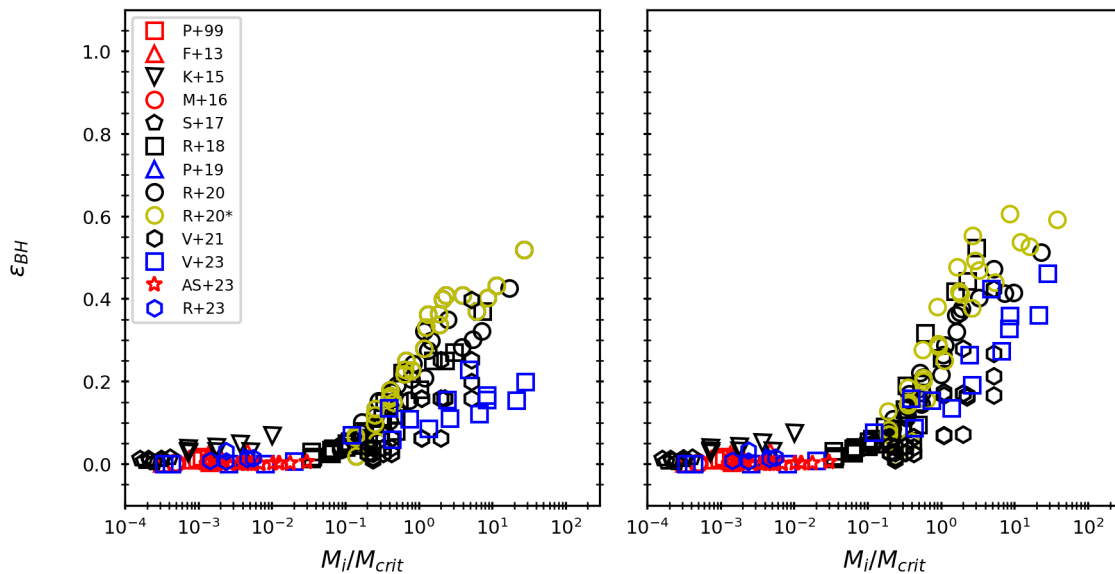


Fig. 1. Black hole formation efficiency, ϵ_{BH} , (left) computed by Eq. 3 against the initial mass of the cluster, M_i , normalized by the critical mass, M_{crit} , calculated via Eq. 1. Different types of star clusters are represented by distinct colors: black symbols for the first star clusters (yellow symbols data from Reinoso et al. (2020), represent models with external potential, calculated via Eq. 2.), red symbols for GCs and blue symbols for NSCs. The final stellar mass is estimated neglecting mass loss via Eq. 4. Right: The black hole formation efficiency ϵ_{BH} computed by Eq. 3 against the current mass of the cluster, M_i , normalized by the critical mass, M_{crit} , calculated from Eq. 1, including an approximate correction for mass loss.

reasons: a) if the mass of the most massive object increases with M_i/M_{crit} as indicated via Fig. 1, this would imply such a relation even in the absence of escapers; b) escapers occur due to interactions within the stellar system and a higher ratio of M_i/M_{crit} implies that such interactions should be more frequent. In the appendix, we examine the dependence between these quantities both for the case when escapers are neglected (as when employing Eq. (4)) and when the full information from the simulations is being employed. We derived a correction factor α (Eq. B.4) to estimate the expected mass loss due to escapers. Of course, we note that the exact volume of mass loss may depend on more factors including the adopted density profile and so the estimate arrived here can at best serve as an approximation.

Applying this correction factor may then lead to an improved estimate of the final stellar mass, M_f , and an improved calculation of ϵ_{BH} . The result of this calculation is given in the right panel of Fig. 1. The behavior is qualitatively similar to what is seen in the previous plot, but overall it appears more pronounced. The efficiency parameter ϵ_{BH} now reaches up to 60% for $M_i/M_{\text{crit}} \gtrsim 1$, although this may also have more moderate

values, on the order of 30 – 40%. An increase in the efficiency already appears visible from $M_i/M_{\text{crit}} \gtrsim 0.1$. For lower values of that ratio, the results appear very similar as before with efficiencies at best on the percent level. Therefore, the critical mass scale is probably not the only factor regulating the efficiency of collisions, although it still appears to be a very important component regulating this process.

3.2. Observational data

For observations, as already noted above, we input the current conditions of the stellar system including M_f and M_{BH} , allowing for the direct calculation of ϵ_{BH} . However, it is to be noted that the initial properties for observational data are more uncertain as in the case of simulations, which are meant to model ideal and isolated systems; real stellar clusters may not be isolated and some of them (particularly the NSCs) may even experience recent or ongoing stellar formation and/or mergers with GCs. It is thus a relevant caveat that needs to be taken (at least for the NSCs), namely, that the evolutionary history, including mass

evolution, will be more complex as compared to the simulations. As discussed already in Section 2.3, for NSCs, we expect and assume an expansion during the evolution, while GCs are typically assumed to have approximately constant radii. However, we note that the half-mass radius could increase by a factor of 2 – 3 during the evolution (Gieles et al. 2010). The situation of UCDs is less clear and thus, we consider two possible scenarios below. To estimate the initial mass for observations, we can consider it as the sum of the current stellar mass and black hole mass it contains, under the assumption that at least its order of magnitude will be similar to M_i/M_{crit} for simulations. The results are shown in Fig. 2. The scatter in this figure is somewhat increased, which given the previous considerations is perhaps unsurprising. Nonetheless, we note that for $M_i/M_{crit} \gtrsim 0.03$, ϵ_{BH} is covering the entire range of efficiencies from the percent level up to $\sim 60\%$. On the other hand, for low values of M_i/M_{crit} , we only have efficiencies of up to 20% at most. In the case of UCDs, we explore one scenario (UCD1), where they are assumed to have fixed radius during their evolution and considering an external potential with 80% of dark matter due to the observed mass to high ratios (e.g., Baumgardt & Mieske 2008). We also explore another case (UCD2), more compatible with Fellhauer & Kroupa (2006), in the absence of dark matter. There, we assume that an initial expansion of the systems takes place, as in the case of NSCs. We find that the case of UCD2 in particular fits very well into the picture and displays a quite similar behavior as the NSCs. The assumptions made in the case of UCD1 would somewhat enhance the scatter, whereas it does not fundamentally change the picture. We also note that high efficiencies close to 100% are only found when the ratio of stellar mass over critical mass is above 1; otherwise, it typically ranges from low efficiencies up to the order of 20%. We further note that we do not know the physics of how the massive black holes in these systems have formed, as it is at least conceivable that also gas physics should have been involved. The latter may contribute to adding scatter in the plot and increase the efficiencies above the expectation from a purely collisional channel. In particular, when considering the group of GCs, we note that they all behave very similarly; in terms of the physics, it is perhaps also the case that is most clear, as they are expected to evolve essentially in isolation after their initial formation. On the other hand, the NSCs are very likely the most complex systems we consider here, with possibly different formation histories, their contribution very considerably increases the scatter we find in this plot. Thus, the UCDs might be somewhere in between GCs and NSCs judging from their respective scatter within the plot.

To assess the sensitivity of this plot to the aforementioned assumptions, we estimated M_i as the sum of the current stellar mass and mass of the black hole within. The critical mass range varies depending on the stellar system age and their initial properties. For NSCs, it typically falls within $10^5 - 10^9 M_\odot$, for GCs, it is between $10^6 - 10^8 M_\odot$, and for UCDs, it ranges from $10^9 - 10^{11} M_\odot$ (UCD1) or $10^7 - 10^9 M_\odot$ (UCD2). The results given in Fig. 2 are in particular overall very similar to the left panel of Fig. 1. We note that for low values of M_i/M_{crit} , efficiencies can reach at best up to 20%, while for $M_i/M_{crit} \gtrsim 0.03$ the whole range of efficiencies up to 100% is possible. Our qualitative conclusions are thus similar though the evolutionary history is more complex as compared to the simulations.

We note three special cases: VCC1254, which introduces a higher scatter at $M_i/M_{crit} \sim 10^{-2}$, with ϵ_{BH} values around 50%. However, the black hole mass of VCC1254 is an upper limit. Besides having a larger nuclear mass-to-light ratio, which means that it must contain an older stellar population (Geha et al. 2002),

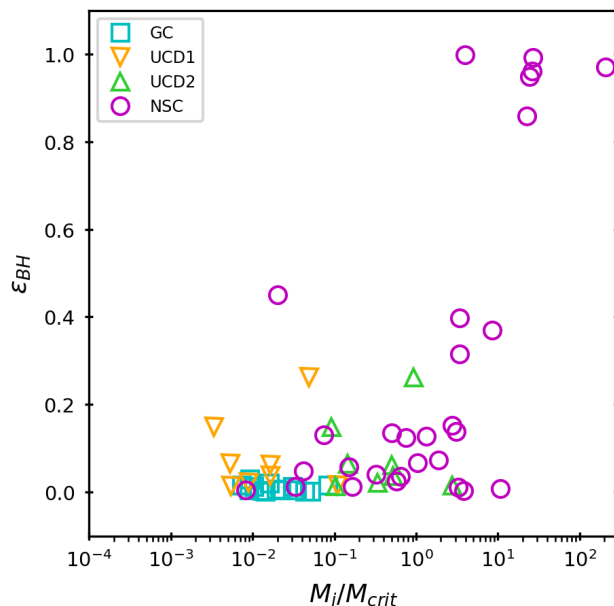


Fig. 2. Black hole formation efficiency, ϵ_{BH} , computed via Eq. 3 against the initial mass of the cluster normalized by the critical mass, M_{crit} (estimated from the current properties of the cluster), for observational data.

in contrast to observations by Durrell (1997) and Stiavelli et al. (2001), which show the presence of young stars. Thus more precise measurements will lead to a more accurate determination of the mass and thus lower ϵ_{BH} . The UCDs M60-UCD1 and UCD320 show $\epsilon_{BH} \approx 15-30\%$ at $M_i/M_{crit} \sim 10^{-3}-10^{-2}$, respectively, under the assumptions of UCD1. Compared to the stellar mass, its high black hole mass suggests that its origin could be a tidal core of a dwarf galaxy (Bassino et al. 1994; Bekki & Freeman 2003; Pfeffer & Baumgardt 2013; Seth et al. 2014; Afanasiev et al. 2018), which aligns with the case of UCD2. Finally, the scatter presented in some observations must be related to their complex formation history, which is beyond the scope of this investigation.

Finally we also note the case of ω Cen (NGC 5139). This GC has been widely studied due to its unique characteristic of being the most massive GC of the Milky Way. Several studies have suggested that the stellar dynamics in ω Cen could be explained due to the presence of an IMBH with a mass $\sim 4 \times 10^4 M_\odot$ at the center (Noyola et al. 2008; Noyola & Baumgardt 2011; Jalali et al. 2012; Baumgardt 2017). Others have argued that the stellar kinematics can be explained by the presence of a dense cluster of stellar-mass black holes (Baumgardt et al. 2019; Zocchi et al. 2019). Other studies suggest that the presence of an IMBH is not necessary to explain the stellar dynamics (van der Marel & Anderson 2010). In this investigation, we consider the first option to determine an upper limit for the efficiency. We note that for the other two options, the black hole formation efficiency will be $\epsilon_{BH} \approx 0$, as this result still aligns with the trend.

3.3. Comparative analysis of observational data and simulations data

So far, we have independently analyzed the data from simulations and observations to check whether they support the concept of a critical mass that significantly determines the efficiency of

collisions in dense stellar systems. We have noted the main differences regarding the typical data that are reported for the respective simulations and observations and developed the tools to at least approximately estimate the quantities that cannot be directly inferred. During the analysis of the observational data, we further encountered some of the systematic differences between simulations that usually model idealized and isolated stellar systems. However, real stellar systems, in particular NSCs, are likely more complex due to their star formation histories as well as occasional mergers with GCs. On the other hand, the GCs appear to at least more closely resemble the behavior of an isolated system as their star formation terminated very long ago, while UCDs are somewhat more uncertain as their origin is not known.

With these differences in mind, we aim to approximately assess what simulations and observations may have in common and which differences can be identified from the comparison. This may, on one hand, allow us to establish processes that play an important role in both observations and simulations, but also help to identify processes that are not yet included in simulations, which may play a possibly important role during their dynamical evolution.

For this analysis here, in the context of the simulations, the mass loss will be estimated using a correction factor, α , (see Eq. B.4) when calculating ϵ_{BH} . In the observations, we have all the information on the current stage. The result of this calculation is given in Fig. 3, where the top panel shows the data comparing all simulations and observations, while in the mid and bottom panels, we focus on data (simulations and observations) for NSCs and GCs, respectively. We note that in the mid panel, we add observations of UCDs, under the assumption of no dark matter but expansion (UCD2), while in the bottom panel, we add observations of UCDs, under the assumption of the presence of dark matter and no expansion (UCD1).

In general, there is a broad consistency between the data from simulations and observations. Where the efficiencies are on the percent level when we consider M_i/M_{crit} to be low, and only for $M_i/M_{\text{crit}} \geq 0.1$ we find higher efficiencies up to of the order 100%, but with significant scatter. Part of the scatter arises from the NSCs for the reasons we were discussing above, namely, the complex star formation histories and mergers with other stellar systems. If we consider globular cluster systems, the simulations and observations appear very consistent and form a tight relation with efficiencies on the percent level at best. The UCDs are most uncertain, while the case of UCD2 (no dark matter, including expansion) fits best within the general trend, also the assumptions of UCD1 (dark matter, no expansion) fit into the general picture. We also emphasize that due to the unclear origin and the complex physics in these systems, a complete agreement could also be coincidental.

4. Summary and conclusions

In this paper, we investigate how the efficiency of black hole formation via collisions in stellar systems depends on the ratio of stellar over critical mass. The importance of the collision timescale in the formation of runaway massive objects has previously been suggested through an analysis of observational properties of both NSCs and massive black holes by Escala (2021), from the comparison of collision timescales with ages in galactic nuclei. The scenario was further tested with satisfactory results, using a set of idealized N-body simulations employing constant stellar masses by Vergara et al. (2023), where a critical mass

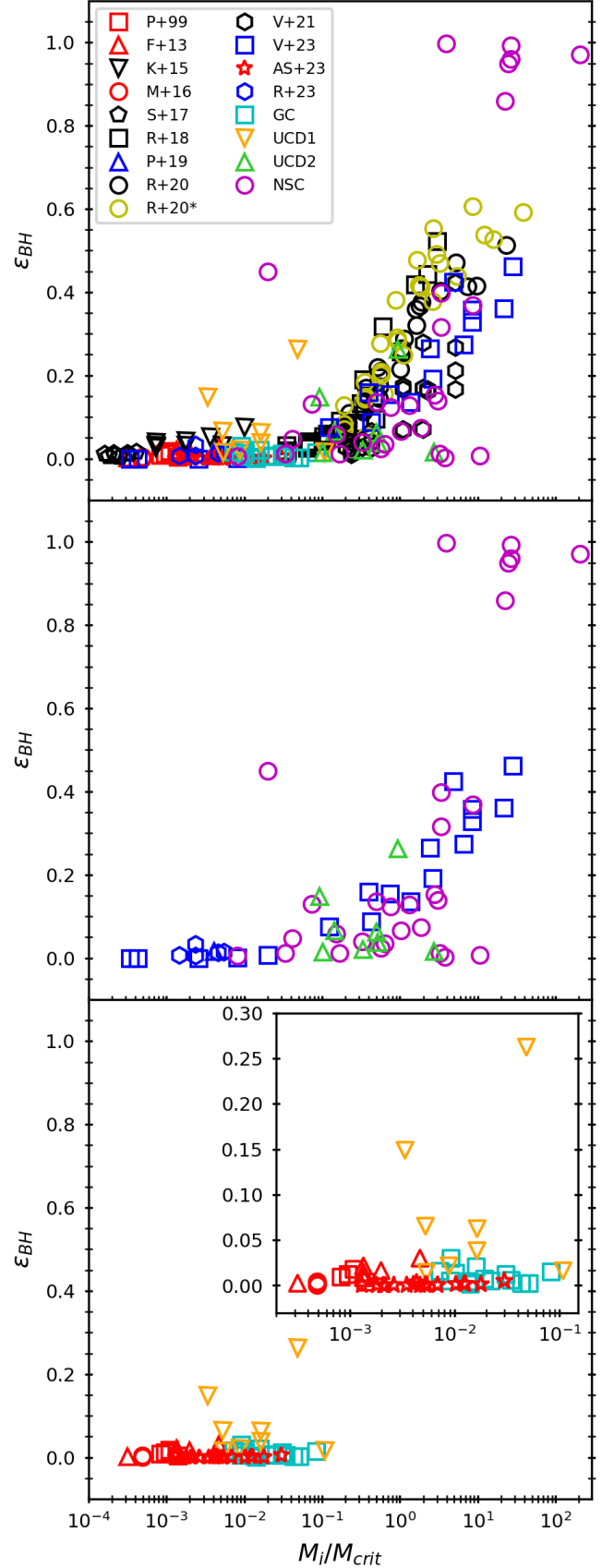


Fig. 3. Black hole formation efficiency ϵ_{BH} computed by Eq. 3 against the current mass of the cluster M_i normalized by the critical mass M_{crit} (Eq. 1) for all observations and simulations (top); for observations and simulations of NSC, also including observations of UCD2 (middle); and for observations and simulations of GC, also including observations of UCD1 (bottom).

for collisions was introduced for the comparison of the collision time with the age of the system.

Here, we have generalized this concept to take into account the presence of an external potential and we employed the result from a large range of numerical simulations and observational data from the literature. This way we compared with the previous results and determined how the efficiency for the formation of massive objects depends on the ratio of initial stellar mass over the critical mass scale defined in Eq. 2. This included simulations with different types of radial profiles in their initial conditions (e.g., [Plummer 1911](#); [King 1966](#); [Miyamoto & Nagai 1975](#)), simulations employing different stellar IMFs (e.g., [Salpeter 1955](#); [Scalo 1986](#); [Kroupa 2001](#)) as well as simulations including stellar evolution ([Hurley et al. 2000, 2002](#)) and simulations with one million stars ([Panamarev et al. 2019](#); [Arca Sedda et al. 2023a,b,c](#)).

The comparison of these data is not completely trivial, for example, not all the output is always reported in the literature; also, while the initial conditions are usually well-described, the final stellar mass in the cluster and the mass loss due to escapers are not always given, but this still forms an important ingredient in our efficiency parameter, ϵ_{BH} . Nonetheless, even under the simplifying assumption that mass loss would be negligible, our analysis has shown a clear correlation between the efficiency required to form a massive object and the ratio of initial stellar mass over critical mass. Particularly, when that ratio is larger than 1, the typical efficiencies lie at least in the range of 20 – 50%; whereas for lower ratios, the most frequent outcome is within the percent range. We note that there is scatter in this relation and we also note some differences in the different sets of simulations, which are also unsurprising given the different assumptions involved. We further note that the obtained correlation improves if we derive a correction factor from the simulations of [Reinoso et al. \(2020\)](#); [Vergara et al. \(2021, 2023\)](#), as for those simulations, we know the fraction of stellar mass lost due to escapers. Assuming that the physics are similar in other simulations, the correlation becomes more clear and we find efficiencies of 20 – 60% when the ratio of initial stellar over critical mass is greater than 1.

Subsequently, we have analyzed observational data of dense stellar systems, including GCs, NSCs, and UCDs. The GCs are perhaps the clearest case as these are very old systems without any recent star formation and where the general evolution is very well understood. For these cases, the ratio of initial stellar over critical mass is in the range of 0.005–0.03 and the efficiencies are very low $\sim 5\%$. The simulations of [Portegies Zwart et al. \(1999\)](#); [Fujii & Portegies Zwart \(2013\)](#); [Mapelli \(2016\)](#) and [Arca Sedda et al. \(2023a,b,c\)](#) show low ϵ_{BH} and further substantiated by observation of [Harris \(e.g 1996\)](#) and [Lützgendorf et al. \(e.g 2011, 2013a,b,c\)](#). This supports the scenario of IMBHs formation in GCs.

In the case of NSCs, we notice more scatter, as the systems are more complex including complicated star formation histories and typically also mergers with other stellar systems. They cover a wide range of initial over critical mass ratios of 0.01 – 100 and, despite the presence of scatter, it is visible that very high efficiencies above 50% are only reached for mass ratios above 0.3.

The UCDs are perhaps the most uncertain systems, as their nature and evolution are not fully clear. We have explored assumptions of these systems both assuming an evolution more like a NSCs and alternatively using an evolutionary path with a fixed radius but including an external potential due to dark matter. The first case is more favorable, while the second somewhat

increases the scatter, although neither of these cases fundamentally change the picture. However, it is noticeable that the observational data do include more scatter than the simulations. This could be due to the higher complexity of those systems in general. Also, it is certainly not guaranteed that the observed systems formed just as a result of collisions, but it could be the case that additional gas physics was also involved, which could help to increase the efficiency with respect to forming a massive object (e.g., [Schleicher et al. 2022](#)).

Overall, while it is clear that additional factors such as the complex history in real stellar systems and the possible presence of gas most likely have an influence on the results and may also be able to explain the scatter that we observe, we find efficiencies of 30 – 100%; these results are correlated with ratios of initial stellar over critical mass above 1. Observations reach higher efficiencies due to the secular evolutionary process of evaporation of the cluster. This result should not be particularly surprising, as it only means that the collision timescale should be short enough to play a relevant role within a given stellar system, but should be useful to determine the potential of a system to form very massive objects. It is worth stressing that high efficiencies can be reached for a wide range of systems. This opens up the potential to form quite massive black holes via the collision channel in massive NSCs, as long as their stellar mass is larger than their critical mass.

In the future, it will be useful for this scenario to be tested further. For example, there are only a few N-body simulations with one million stars available, such as those of [Panamarev et al. \(2019\)](#); [Arca Sedda et al. \(2023a,b,c\)](#). More simulations and more compact systems will allow us to test this scenario further and under more realistic conditions. At the same time, the complexity of simulations could still be increased, by implementing ongoing star formation as expected within real NSCs and/or mergers with GCs as another possible growth channel. To understand the importance of this black hole formation mechanism, statistical predictions will be important in combining semi-analytic galaxy evolution models, as those of [Sassano et al. \(e.g. 2021\)](#); [Trinca et al. \(e.g. 2022\)](#), with black hole formation recipes employing the concept of the critical mass scale to obtain statistical predictions at both high and low redshift. In the Local Universe, such predictions could be compared to the black hole mass function determined via the [James Webb Space Telescope \(JWST\)](#) and the [Extremely Large Telescope \(ELT\)](#), where new IMBHs may be discovered at the lower mass end and in general more data will become available for testing the scenario proposed here. At high redshift, this scenario can operate and its relevance for the formation of high redshift black holes needs to be further explored.

While the potential importance of the collision-based channels for black hole formation has already been suggested by [Rees \(1984\)](#), previous estimates typically insinuate that they form black hole masses up to the order of $10^3 M_{\odot}$ (e.g., [Devecchi & Volonteri 2009](#); [Devecchi et al. 2010](#); [Katz et al. 2015](#); [Sakurai et al. 2017](#); [Reinoso et al. 2018](#)). The results obtained here considerably strengthen and support the relevance of the collision-based channel, suggesting that it could efficiently operate in dense NSCs and the efficiency of SMBH formation in typical NSCs appears roughly consistent with this scenario, including SMBH masses on the order of $10^6 M_{\odot}$ and somewhat above. It is even further consistent with the very low efficiencies in GCs, while the results for UCDs are not fully conclusive, as they depend on certain assumptions being made concerning these objects. What we can conclude from the comparison with the large set of simulations analyzed in this work is that the sce-

nario holds over a wide range of possible conditions, including variations of the radial profile of the clusters, the presence of an initial mass function, and the inclusion of additional physics such as stellar evolution. Future simulations with high particle numbers and exploring additional physics, including improved treatments of collisions and stellar physics (e.g., [Kamlah et al. 2024](#)), and investigating the role of rotation and binaries will allow us to probe this scenario in even greater detail.

Acknowledgements. We thank the anonymous referee for his/her comments, which helped to improve the manuscript quality. MCV acknowledges funding through ANID (Doctorado acuerdo bilateral DAAD/62210038) and DAAD (funding program number 57600326). DRGS, AE and ML acknowledge the center for Astrophysics and Associated Technologies CATA (FB210003) and via ANID Fondo 2022 QUIMAL 220002. DRGS and ML also acknowledge financial support from FONDECYT Regular grant #1201280 and through the Alexander von Humboldt - Foundation, Bonn, Germany. BR acknowledges funding through ANID (CONICYT-PFCHA/Doctorado acuerdo bilateral DAAD/62180013), DAAD (funding program number 57451854), and the International Max Planck Research School for Astronomy and Cosmic Physics at the University of Heidelberg (IMPRS-HD). FFD, AWHK, and RS acknowledge financial support by German Science Foundation (DFG) project Sp 345/22-1 and Sp 345/24-1. Computations were performed on the HPC system Raven at the Max Planck Computing and Data Facility, and we also acknowledge the Gauss center for Supercomputing e.V. for computing time through the John von Neumann Institute for Computing (NIC) on the GCS Supercomputer JUWELS Booster at Jülich Supercomputing center (JSC). These resources made the presented work possible, by supporting its development. NH is a fellow of the International Max Planck Research School for Astronomy and Cosmic Physics at the University of Heidelberg (IMPRS-HD). NH acknowledges funding through [LACEGAL](#), a Latinamerican Chinese European Galaxy Formation Network. This project has received funding from the European Union's HORIZON-MSCA-2021-SE-01 Research and Innovation programme under the Marie Skłodowska-Curie grant agreement number 101086388.

References

- Aarseth, S. J. 1999a, *PASP*, 111, 1333
Aarseth, S. J. 1999b, *Celestial Mechanics and Dynamical Astronomy*, 73, 127
Aarseth, S. J. 2000, in *The Chaotic Universe*, ed. V. G. Gurzadyan & R. Ruffini, 286–287
Afanasyev, A. V., Chilingarian, I. V., Mieske, S., et al. 2018, *MNRAS*, 477, 4856
Aharon, D. & Perets, H. B. 2015, *ApJ*, 799, 185
Ahmad, A. & Cohen, L. 1973, *Journal of Computational Physics*, 12, 389
Ahn, C. P., Seth, A. C., Cappellari, M., et al. 2018, *ApJ*, 858, 102
Ahn, C. P., Seth, A. C., den Brok, M., et al. 2017, *ApJ*, 839, 72
Arca-Sedda, M. & Capuzzo-Dolcetta, R. 2014, *MNRAS*, 444, 3738
Arca Sedda, M., Kamlah, A. W. H., Spurzem, R., et al. 2023a, *arXiv e-prints*, arXiv:2307.04805
Arca Sedda, M., Kamlah, A. W. H., Spurzem, R., et al. 2023b, *arXiv e-prints*, arXiv:2307.04806
Arca Sedda, M., Kamlah, A. W. H., Spurzem, R., et al. 2023c, *arXiv e-prints*, arXiv:2307.04807
Ashok, A., Seth, A., Erwin, P., et al. 2023, *ApJ*, 958, 100
Bañados, E., Venemans, B. P., Decarli, R., et al. 2016, *ApJS*, 227, 11
Banerjee, S. & Kroupa, P. 2017, *A&A*, 597, A28
Barber, J., Chattopadhyay, D., & Antonini, F. 2024, *MNRAS*, 527, 7363
Barnes, J. & Hut, P. 1986, *Nature*, 324, 446
Barnes, J. E. 2002, *MNRAS*, 333, 481
Barnes, J. E. & Hernquist, L. E. 1991, *ApJ*, 370, L65
Barth, A. J., Strigari, L. E., Bentz, M. C., Greene, J. E., & Ho, L. C. 2009, in *American Astronomical Society Meeting Abstracts*, Vol. 214, American Astronomical Society Meeting Abstracts #214, 419.09
Bassino, L. P., Muzzio, J. C., & Rabolli, M. 1994, *ApJ*, 431, 634
Baumgardt, H. 2017, *MNRAS*, 464, 2174
Baumgardt, H., He, C., Sweet, S. M., et al. 2019, *MNRAS*, 488, 5340
Baumgardt, H. & Mieske, S. 2008, *MNRAS*, 391, 942
Bekki, K. & Freeman, K. C. 2003, *MNRAS*, 346, L11
Blum, R. D., Sellgren, K., & Depoy, D. L. 1996, *ApJ*, 470, 864
Blumenthal, K. A. & Barnes, J. E. 2018, *MNRAS*, 479, 3952
Boekholt, T. C. N., Schleicher, D. R. G., Fellhauer, M., et al. 2018, *MNRAS*, 476, 366
Böker, T. 2008, in *Journal of Physics Conference Series*, Vol. 131, *Journal of Physics Conference Series*, 012043
Böker, T. 2010, in *Star Clusters: Basic Galactic Building Blocks Throughout Time and Space*, ed. R. de Grijs & J. R. D. Lépine, Vol. 266, 58–63
Böker, T., Laine, S., van der Marel, R. P., et al. 2002, *AJ*, 123, 1389
Böker, T., van der Marel, R. P., & Vacca, W. D. 1999, *AJ*, 118, 831
Bromm, V. & Loeb, A. 2003, *ApJ*, 596, 34
Cappellari, M., Bertola, F., Burstein, D., et al. 1999, *ApJ*, 515, L17
Chen, K.-J., Heger, A., Woosley, S., Almgren, A., & Whalen, D. J. 2014, *ApJ*, 792, 44
Chilingarian, I. V. & Mamon, G. A. 2008, *MNRAS*, 385, L83
Chilingarian, I. V., Mieske, S., Hilker, M., & Infante, L. 2011, *MNRAS*, 412, 1627
Chon, S. & Omukai, K. 2020, *MNRAS*, 494, 2851
Coccatto, L., Morelli, L., Pizzella, A., et al. 2013, *A&A*, 549, A3
Côté, P., Piatek, S., Ferrarese, L., et al. 2006, *ApJS*, 165, 57
Dabringhausen, J., Fellhauer, M., & Kroupa, P. 2010, *MNRAS*, 403, 1054
Dabringhausen, J., Kroupa, P., & Baumgardt, H. 2009, *MNRAS*, 394, 1529
Das, A., Schleicher, D. R. G., Leigh, N. W. C., & Boekholt, T. C. N. 2021, *MNRAS*, 503, 1051
Davidge, T. J. 2003, *ApJ*, 597, 289
Davis, T. A., Nguyen, D. D., Seth, A. C., et al. 2020, *MNRAS*, 496, 4061
De Angeli, F., Piotto, G., Cassisi, S., et al. 2005, *AJ*, 130, 116
den Brok, M., Seth, A. C., Barth, A. J., et al. 2015, *ApJ*, 809, 101
Devecchi, B. & Volonteri, M. 2009, *ApJ*, 694, 302
Devecchi, B., Volonteri, M., Colpi, M., & Haardt, F. 2010, *MNRAS*, 409, 1057
Do, T., Hees, A., Ghez, A., et al. 2019, *Science*, 365, 664
Durrell, P. R. 1997, *AJ*, 113, 531
Eggleton, P. P. & Tout, C. A. 1989, *Space Sci. Rev.*, 50, 165
Elmegreen, B. G., Bournaud, F., & Elmegreen, D. M. 2008, *ApJ*, 684, 829
Emsellem, E., Dejonghe, H., & Bacon, R. 1999, *MNRAS*, 303, 495
Escala, A. 2006, *ApJ*, 648, L13
Escala, A. 2007, *ApJ*, 671, 1264
Escala, A. 2021, *ApJ*, 908, 57
Event Horizon Telescope Collaboration, Akiyama, K., Alberdi, A., et al. 2022, *ApJ*, 930, L12
Fahrión, K., Georgiev, I., Hilker, M., et al. 2019, *A&A*, 625, A50
Faifer, F. R., Escudero, C. G., Scalia, M. C., et al. 2017, *A&A*, 599, L8
Fan, X., Bañados, E., & Simcoe, R. A. 2023, *ARA&A*, 61, 373
Fan, X., Strauss, M. A., Schneider, D. P., et al. 2003, *AJ*, 125, 1649
Feldmeier, A., Lützgendorf, N., Neumayer, N., et al. 2013, *A&A*, 554, A63
Fellhauer, M., Baumgardt, H., Kroupa, P., & Spurzem, R. 2002, *Celestial Mechanics and Dynamical Astronomy*, 82, 113
Fellhauer, M. & Kroupa, P. 2002, *MNRAS*, 330, 642
Fellhauer, M. & Kroupa, P. 2006, *MNRAS*, 367, 1577
Ferrarese, L., Côté, P., Dalla Bontà, E., et al. 2006, *ApJ*, 644, L21
Ferrarese, L. & Merritt, D. 2000, *ApJ*, 539, L9
Francis, K. J., Drinkwater, M. J., Chilingarian, I. V., Bolt, A. M., & Firth, P. 2012, *MNRAS*, 425, 325
Fritz, T. K., Chatzopoulos, S., Gerhard, O., et al. 2016, *ApJ*, 821, 44
Fujii, M., Iwasawa, M., Funato, Y., & Makino, J. 2007, *PASJ*, 59, 1095
Fujii, M. S. & Portegies Zwart, S. 2013, *MNRAS*, 430, 1018
Fusco, M. S., Davis, B. L., Kenefick, J., Kenefick, D., & Seigar, M. S. 2022, *Universe*, 8, 649
Gebhardt, K., Adams, J., Richstone, D., et al. 2011, *ApJ*, 729, 119
Gebhardt, K., Lauer, T. R., Kormendy, J., et al. 2001, *AJ*, 122, 2469
Gebhardt, K., Rich, R. M., & Ho, L. C. 2005, *ApJ*, 634, 1093
Gebhardt, K., Richstone, D., Tremaine, S., et al. 2003, *ApJ*, 583, 92
Geha, M., Guhathakurta, P., & van der Marel, R. P. 2002, *AJ*, 124, 3073
Genzel, R., Eisenhauer, F., & Gillessen, S. 2010, *Reviews of Modern Physics*, 82, 3121
Georgiev, I. Y., Böker, T., Leigh, N., Lützgendorf, N., & Neumayer, N. 2016, *MNRAS*, 457, 2122
Georgiev, I. Y., Hilker, M., Puzia, T. H., Goudfrooij, P., & Baumgardt, H. 2009, *MNRAS*, 396, 1075
Gerssen, J., van der Marel, R. P., Gebhardt, K., et al. 2002, *AJ*, 124, 3270
Ghez, A. M., Salim, S., Weinberg, N. N., et al. 2008, *ApJ*, 689, 1044
Gieles, M., Baumgardt, H., Heggge, D. C., & Lamers, H. J. G. L. M. 2010, *MNRAS*, 408, L16
Gillessen, S., Plewa, P. M., Eisenhauer, F., et al. 2017, *ApJ*, 837, 30
Gnedin, O. Y., Ostriker, J. P., & Tremaine, S. 2014, *ApJ*, 785, 71
Graham, A. W. 2008, *PASA*, 25, 167
Graham, A. W. & Spitler, L. R. 2009, *MNRAS*, 397, 2148
GRAVITY Collaboration, Abuter, R., Amorim, A., et al. 2018, *A&A*, 615, L15
Gültekin, K., Richstone, D. O., Gebhardt, K., et al. 2009, *ApJ*, 698, 198
Haemmerlé, L., Woods, T. E., Klessen, R. S., Heger, A., & Whalen, D. J. 2018, *MNRAS*, 474, 2757
Häring, N. & Rix, H.-W. 2004, *ApJ*, 604, L89
Harris, W. E. 1996, *AJ*, 112, 1487
Heger, A. & Woosley, S. E. 2002, *ApJ*, 567, 532
Hosokawa, T., Omukai, K., & Yorke, H. W. 2012, *ApJ*, 756, 93
Hosokawa, T., Yorke, H. W., Inayoshi, K., Omukai, K., & Yoshida, N. 2013, *ApJ*, 778, 178
Hurley, J. R., Pols, O. R., & Tout, C. A. 2000, *MNRAS*, 315, 543

- Hurley, J. R., Tout, C. A., & Pols, O. R. 2002, *MNRAS*, 329, 897
- Ibata, R., Bellazzini, M., Chapman, S. C., et al. 2009, *ApJ*, 699, L169
- Jalali, B., Baumgardt, H., Kissler-Patig, M., et al. 2012, *A&A*, 538, A19
- Jeram, S., Gonzalez, A., Eikenberry, S., et al. 2020, *ApJ*, 899, 76
- Kacharov, N., Neumayer, N., Seth, A. C., et al. 2018, *MNRAS*, 480, 1973
- Kamlah, A. W. H., Leveque, A., Spurzem, R., et al. 2022, *MNRAS*, 511, 4060
- Kamlah, A. W. H., Spurzem, R., Arca Sedda, M., et al. 2024, *MNRAS*, in prep. [arXiv:2212.06907]
- Katz, H., Sijacki, D., & Haehnelt, M. G. 2015, *MNRAS*, 451, 2352
- King, A. 2016, *MNRAS*, 456, L109
- King, I. R. 1966, *AJ*, 71, 64
- Kinoshita, H., Yoshida, H., & Nakai, H. 1990, *Celestial Mechanics and Dynamical Astronomy*, 50, 59
- Koliopoulos, F. 2017, in *XII Multifrequency Behaviour of High Energy Cosmic Sources Workshop (MULTIF2017)*, 51
- Kormendy, J., Drory, N., Bender, R., & Cornell, M. E. 2010, *ApJ*, 723, 54
- Kormendy, J. & Ho, L. C. 2013, *ARA&A*, 51, 511
- Krajinović, D., Cappellari, M., McDermid, R. M., et al. 2018, *MNRAS*, 477, 3030
- Kravtsov, A. V. & Gnedin, O. Y. 2005, *ApJ*, 623, 650
- Kroupa, P. 1998, *MNRAS*, 300, 200
- Kroupa, P. 2001, *MNRAS*, 322, 231
- Kruijssen, J. M. D., Pfeffer, J. L., Reina-Campos, M., Crain, R. A., & Bastian, N. 2019, *MNRAS*, 486, 3180
- Latif, M. A. & Schleicher, D. R. G. 2015, *A&A*, 578, A118
- Latif, M. A., Schleicher, D. R. G., Bovino, S., Grassi, T., & Spaans, M. 2014, *ApJ*, 792, 78
- Latif, M. A., Schleicher, D. R. G., Schmidt, W., & Niemeyer, J. C. 2013, *MNRAS*, 436, 2989
- Lee, H. M. 1987, *ApJ*, 319, 801
- Liu, S., Wang, L., Hu, Y.-M., Tanikawa, A., & Trani, A. A. 2023, arXiv e-prints, arXiv:2311.05393
- Lützgendorf, N., Kissler-Patig, M., Gebhardt, K., et al. 2013a, *A&A*, 552, A49
- Lützgendorf, N., Kissler-Patig, M., Gebhardt, K., et al. 2012, *A&A*, 542, A129
- Lützgendorf, N., Kissler-Patig, M., Neumayer, N., et al. 2013b, *A&A*, 555, A26
- Lützgendorf, N., Kissler-Patig, M., Neumayer, N., et al. 2013c, *A&A*, 555, A26
- Lützgendorf, N., Kissler-Patig, M., Noyola, E., et al. 2011, *A&A*, 533, A36
- Ma, J., de Grijs, R., Chen, D., et al. 2007, *MNRAS*, 376, 1621
- Machida, M. N. & Doi, K. 2013, *MNRAS*, 435, 3283
- Magorrian, J., Tremaine, S., Richstone, D., et al. 1998, *AJ*, 115, 2285
- Makino, J. 2004, *PASJ*, 56, 521
- Mapelli, M. 2016, *MNRAS*, 459, 3432
- Marconi, A. & Hunt, L. K. 2003, *ApJ*, 589, L21
- Mayer, L., Kazantzidis, S., Escala, A., & Callegari, S. 2010, *Nature*, 466, 1082
- McConnell, N. J., Ma, C.-P., Gebhardt, K., et al. 2011, *Nature*, 480, 215
- McLaughlin, D. E., King, A. R., & Nayakshin, S. 2006, *ApJ*, 650, L37
- McMillan, S. L. W. 1996, in *Astronomical Society of the Pacific Conference Series*, Vol. 90, *The Origins, Evolution, and Destinies of Binary Stars in Clusters*, ed. E. F. Milone & J. C. Mermilliod, 413
- Mehrgan, K., Thomas, J., Saglia, R., et al. 2019, *ApJ*, 887, 195
- Merritt, D., Ferrarese, L., & Joseph, C. L. 2001, *Science*, 293, 1116
- Meylan, G., Sarajedini, A., Jablonka, P., et al. 2001, *AJ*, 122, 830
- Mikkola, S. & Aarseth, S. J. 1990, *Celestial Mechanics and Dynamical Astronomy*, 47, 375
- Mikkola, S. & Aarseth, S. J. 1993, *Celestial Mechanics and Dynamical Astronomy*, 57, 439
- Miyamoto, M. & Nagai, R. 1975, *PASJ*, 27, 533
- Mortlock, D. J., Warren, S. J., Venemans, B. P., et al. 2011, *Nature*, 474, 616
- Natarajan, P. & Treister, E. 2009, *MNRAS*, 393, 838
- Neumayer, N., Seth, A., & Böker, T. 2020, *A&A Rev.*, 28, 4
- Neumayer, N. & Walcher, C. J. 2012, *Advances in Astronomy*, 2012, 709038
- Newton, R. D. A. & Kay, S. T. 2013, *MNRAS*, 434, 3606
- Nguyen, D. D., Bureau, M., Thater, S., et al. 2022, *MNRAS*, 509, 2920
- Nguyen, D. D., Seth, A. C., den Brok, M., et al. 2017, *ApJ*, 836, 237
- Nguyen, D. D., Seth, A. C., Neumayer, N., et al. 2019, *ApJ*, 872, 104
- Nguyen, D. D., Seth, A. C., Neumayer, N., et al. 2018, *ApJ*, 858, 118
- Nitadori, K. & Makino, J. 2008, *New A*, 13, 498
- Noyola, E. & Baumgardt, H. 2011, *ApJ*, 743, 52
- Noyola, E., Gebhardt, K., & Bergmann, M. 2008, *ApJ*, 676, 1008
- Omukai, K. & Nishi, R. 1998, *ApJ*, 508, 141
- Onken, C. A., Bian, F., Fan, X., et al. 2020, *MNRAS*, 496, 2309
- Ordenes-Briceño, Y., Puzia, T. H., Eigenthaler, P., et al. 2018, *ApJ*, 860, 4
- Pacucci, F., Natarajan, P., & Ferrara, A. 2017, *ApJ*, 835, L36
- Panamarev, T., Just, A., Spurzem, R., et al. 2019, *MNRAS*, 484, 3279
- Paudel, S., Lisker, T., & Kuntschner, H. 2011, *MNRAS*, 413, 1764
- Pechetti, R., Seth, A., Cappellari, M., et al. 2017, *ApJ*, 850, 15
- Pechetti, R., Seth, A., Kamann, S., et al. 2022, *ApJ*, 924, 48
- Pechetti, R., Seth, A., Neumayer, N., et al. 2020, *ApJ*, 900, 32
- Peterson, B. M., Bentz, M. C., Desroches, L.-B., et al. 2005, *ApJ*, 632, 799
- Pfeffer, J. & Baumgardt, H. 2013, *MNRAS*, 433, 1997
- Pfuhl, O., Fritz, T. K., Zilka, M., et al. 2011, *ApJ*, 741, 108
- Plummer, H. C. 1911, *MNRAS*, 71, 460
- Portegies Zwart, S. F., Makino, J., McMillan, S. L. W., & Hut, P. 1999, *A&A*, 348, 117
- Portegies Zwart, S. F. & McMillan, S. L. W. 2002, *ApJ*, 576, 899
- Portegies Zwart, S. F. & Verbunt, F. 1996, *A&A*, 309, 179
- Prieto, J. & Escala, A. 2016, *MNRAS*, 460, 4018
- Prieto, J., Escala, A., Privon, G. C., & d'Etigny, J. 2021, *MNRAS*, 508, 3672
- Quinlan, G. D. & Shapiro, S. L. 1990, *ApJ*, 356, 483
- Rantala, A., Naab, T., Rizzuto, F. P., et al. 2023, *MNRAS*, 522, 5180
- Rantala, A., Naab, T., & Springel, V. 2021, *MNRAS*, 502, 5546
- Rees, M. J. 1984, *ARA&A*, 22, 471
- Regan, J. A., Wise, J. H., Woods, T. E., et al. 2020, *The Open Journal of Astrophysics*, 3, 15
- Reinoso, B., Klessen, R. S., Schleicher, D., Glover, S. C. O., & Solar, P. 2023, *MNRAS*, 521, 3553
- Reinoso, B., Schleicher, D. R. G., Fellhauer, M., Klessen, R. S., & Boekholt, T. C. N. 2018, *A&A*, 614, A14
- Reinoso, B., Schleicher, D. R. G., Fellhauer, M., Leigh, N. W. C., & Klessen, R. S. 2020, *A&A*, 639, A92
- Repetto, P., Faúndez-Abans, M., Freitas-Lemes, P., Rodrigues, I., & de Oliveira-Abans, M. 2017, *MNRAS*, 464, 293
- Riaz, S., Hartwig, T., & Latif, M. A. 2022, *ApJ*, 937, L6
- Ricarte, A. & Natarajan, P. 2018, *MNRAS*, 481, 3278
- Rizzuto, F. P., Naab, T., Rantala, A., et al. 2023, *MNRAS*, 521, 2930
- Rosenberg, A., Saviane, I., Piotto, G., & Aparicio, A. 1999, *AJ*, 118, 2306
- Rossa, J., van der Marel, R. P., Böker, T., et al. 2006, *AJ*, 132, 1074
- Saglia, R. P., Opitsch, M., Erwin, P., et al. 2016, *ApJ*, 818, 47
- Sakurai, Y., Yoshida, N., & Fujii, M. S. 2019, *MNRAS*, 484, 4665
- Sakurai, Y., Yoshida, N., Fujii, M. S., & Hirano, S. 2017, *MNRAS*, 472, 1677
- Salpeter, E. E. 1955, *ApJ*, 121, 161
- Sánchez-Janssen, R., Côté, P., Ferrarese, L., et al. 2019, *ApJ*, 878, 18
- Sarzi, M., Rix, H.-W., Shields, J. C., et al. 2005, *ApJ*, 628, 169
- Sarzi, M., Rix, H.-W., Shields, J. C., et al. 2001, *ApJ*, 550, 65
- Sassano, F., Schneider, R., Valiante, R., et al. 2021, *MNRAS*, 506, 613
- Savorgnan, G. A. D., Graham, A. W., Marconi, A., & Sani, E. 2016, *ApJ*, 817, 21
- Scalo, J. M. 1986, *Fund. Cosmic Phys.*, 11, 1
- Schaerer, D. 1999, in *Wolf-Rayet Phenomena in Massive Stars and Starburst Galaxies*, ed. K. A. van der Hucht, G. Koenigsberger, & P. R. J. Eenens, Vol. 193, 539
- Schleicher, D. R. G., Palla, F., Ferrara, A., Galli, D., & Latif, M. 2013, *A&A*, 558, A59
- Schleicher, D. R. G., Reinoso, B., & Klessen, R. S. 2023, *MNRAS*, 521, 3972
- Schleicher, D. R. G., Reinoso, B., Latif, M., et al. 2022, *MNRAS*, 512, 6192
- Schödel, R., Feldmeier, A., Neumayer, N., Meyer, L., & Yelda, S. 2014, *Classical and Quantum Gravity*, 31, 244007
- Seth, A., Agüeros, M., Lee, D., & Basu-Zych, A. 2008, *ApJ*, 678, 116
- Seth, A. C., van den Bosch, R., Mieske, S., et al. 2014, *Nature*, 513, 398
- Shcherbakov, R. V., Wong, K.-W., Irwin, J. A., & Reynolds, C. S. 2014, *ApJ*, 782, 103
- Shlosman, I., Begelman, M. C., & Frank, J. 1990, *Nature*, 345, 679
- Spitzer, Lyman, J. & Thuan, T. X. 1972, *ApJ*, 175, 31
- Spurzem, R. & Kamlah, A. 2023, *Living Reviews in Computational Astrophysics*, 9, 3
- Stiavelli, M., Miller, B. W., Ferguson, H. C., et al. 2001, *AJ*, 121, 1385
- Stiefel, E. & Kustanheimo, P. 1965, *Journal für die reine und angewandte Mathematik*, 218, 204
- Stone, N. C., Küpper, A. H. W., & Ostriker, J. P. 2017, *MNRAS*, 467, 4180
- Tan, J. C. & McKee, C. F. 2004, *ApJ*, 603, 383
- Thater, S., Krajinović, D., Bourne, M. A., et al. 2017, *A&A*, 597, A18
- Thater, S., Lyubenova, M., Fahrion, K., et al. 2023, *A&A*, 675, A18
- Trager, S. C., Faber, S. M., Worthey, G., & González, J. J. 2000, *AJ*, 119, 1645
- Tremaine, S., Gebhardt, K., Bender, R., et al. 2002, *ApJ*, 574, 740
- Tremaine, S. D., Ostriker, J. P., & Spitzer, L., J. 1975, *ApJ*, 196, 407
- Trinca, A., Schneider, R., Valiante, R., et al. 2022, *MNRAS*, 511, 616
- Turner, M. L., Côté, P., Ferrarese, L., et al. 2012, *ApJS*, 203, 5
- Urrutia Zapata, F., Fellhauer, M., Alarcón Jara, A. G., Matus Carrillo, D. R., & Aravena, C. A. 2019, *MNRAS*, 489, 2746
- van der Marel, R. P. & Anderson, J. 2010, *ApJ*, 710, 1063
- Vergara, M. C., Escala, A., Schleicher, D. R. G., & Reinoso, B. 2023, *MNRAS*, 522, 4224
- Vergara, M. Z. C., Schleicher, D. R. G., Boekholt, T. C. N., et al. 2021, *A&A*, 649, A160
- Villaume, A., Brodie, J., Conroy, C., Romanowsky, A. J., & van Dokkum, P. 2017, *ApJ*, 850, L14
- Vogel, K. T., Seth, A. C., Neumayer, N., et al. 2018, *ApJ*, 858, 20
- Volonteri, M. 2010, *A&A Rev.*, 18, 279
- Volonteri, M., Haardt, F., & Madau, P. 2003, *ApJ*, 582, 559
- Volonteri, M., Lodato, G., & Natarajan, P. 2008, *MNRAS*, 383, 1079

- Walcher, C. J., Böker, T., Charlot, S., et al. 2006, *ApJ*, 649, 692
Walcher, C. J., van der Marel, R. P., McLaughlin, D., et al. 2005, *ApJ*, 618, 237
Wang, F., Yang, J., Fan, X., et al. 2021, *ApJ*, 907, L1
Wang, L., Gieles, M., Baumgardt, H., et al. 2024, *MNRAS*, 527, 7495
Wang, L., Iwasawa, M., Nitadori, K., & Makino, J. 2020, *MNRAS*, 497, 536
Wang, L., Spurzem, R., Aarseth, S., et al. 2016, *MNRAS*, 458, 1450
Wang, L., Spurzem, R., Aarseth, S., et al. 2015, *MNRAS*, 450, 4070
Wang, L., Tanikawa, A., & Fujii, M. 2022, *MNRAS*, 515, 5106
Wehner, E. H. & Harris, W. E. 2006, *ApJ*, 644, L17
Whalen, D. J., Johnson, J. L., Smidt, J., et al. 2013, *ApJ*, 774, 64
White, S. D. M. & Rees, M. J. 1978, *MNRAS*, 183, 341
Wisdom, J. & Holman, M. 1991, *AJ*, 102, 1528
Wu, X.-B., Wang, F., Fan, X., et al. 2015, *Nature*, 518, 512
Wurster, J. & Thacker, R. J. 2013, *MNRAS*, 431, 539
Zocchi, A., Gieles, M., & Hénault-Brunet, V. 2019, *MNRAS*, 482, 4713
Zuo, W., Wu, X.-B., Fan, X., et al. 2015, *ApJ*, 799, 189
Zwick, L., Mayer, L., Haemmerlé, L., & Klessen, R. S. 2023, *MNRAS*, 518, 2076

Appendix A: Computation of the critical mass and black hole formation efficiency for simulations

Fujii & Portegies Zwart (2013) delved into the role of stellar collisions in ensemble star clusters and virialized solo-cluster models. In this work, we focus on the latter. Those authors used a Salpeter (1955) IMF with $M_{\min} = 1M_{\odot}$ and $M_{\max} = 100M_{\odot}$ and density profile of King (1966). To compute the critical mass and the black hole formation efficiency, we used the number of stars (N), the cluster mass (M_i), the half-mass radius, the mean stellar mass ($\overline{m_*} = M_i/N$), and, finally, the black hole mass after a simulation time of 5 Myr. In the study of Sakurai et al. (2017) they explore runaway collisions in the first star cluster, using a Salpeter (1955) IMF varying the masses between 3–100 M_{\odot} . The distribution of stars does not follow any profile mentioned before, since the positions of the stars were obtained from previous hydrodynamics simulations. The parameters adopted to compute the M_{crit} and ϵ_{BH} were the simulation time ($\tau = 3$ Myr), the initial cluster, the number of stars, and the black hole mass.

Portegies Zwart et al. (1999) explored runaway collisions in young compact star clusters. They employed a Scalo (1986) IMF, which varies the stellar mass between 0.1 and 100 M_{\odot} . We used N , $\overline{m_*}$, $M_i = N * \overline{m_*}$, and R_h in addition to the values for the black hole mass and the simulation time (from Figure 2) to compute M_{crit} and ϵ_{BH} . Mapelli (2016) explored the impact of metallicity in runaway collisions in young dense star clusters. The authors used the Kroupa (2001) IMF with $M_{\min} = 0.1M_{\odot}$ and $M_{\max} = 150M_{\odot}$. The parameters used to calculate the critical mass and the black hole formation efficiency are N , M_i , $\overline{m_*} = M_i/N$, and R_h . The stellar system was evolved for over 17 Myr, forming binary systems. We just consider the mass of the most massive one of the binary system. Both works used the King (1966) profile.

Katz et al. (2015) investigated primordial star clusters at high redshift. They modeled both spherical (Plummer 1911) and non-spherical star distributions, but for our purposes, we selected the spherical model due to the availability of the virial radius (R_v). As per its definition, R_v is not available for the non-spherical distribution, rendering it impossible to compute M_{crit} . The study used a (Salpeter 1955) IMF with $M_{\min} = 1 M_{\odot}$ and $M_{\max} = 100 M_{\odot}$. To calculate M_{crit} and ϵ_{BH} , we employed the following parameters R_v , M_i , and M_{BH} , although the value of N is absent, they provided the IMF, which allowed us to calculate the mean stellar mass ($\overline{m_*}$) and subsequently determine the number of stars as $N = M_i/\overline{m_*}$. The simulations run for 3.5 Myr. Reinoso et al. (2018) explored collisions in primordial star clusters. They used equal-mass stars distributed according to a Plummer distribution (Plummer 1911). To estimate ϵ_{BH} and M_{crit} , we used the initial cluster mass and the half-mass radius, the number of stars, the mean stellar mass $\overline{m_*} = M_i/N$, and stellar radii $r_* = 20, 50, 100, 200, 500, 1000, 5000 R_{\odot}$. The larger stellar radii were assumed based on a high accretion rate of $0.1 M_{\odot} \text{ yr}^{-1}$ for the protostars (Hosokawa et al. 2012, 2013; Schleicher et al. 2013; Haemmerlé et al. 2018). Their simulations spanned 2 Myr and resulted in the formation of very massive stars. These simulations do not include stellar evolution, however, if the simulation time is sufficient to form a black hole, then they consider the masses of these very massive stars as the black hole mass. Reinoso et al. (2020) investigated runaway collisions in dense star clusters, considering both the presence and absence of external potential effects. They adopted a star distribution from Plummer (1911) with equal-mass stars. To compute the critical mass, we use Eq. 1 for systems without external potential and Eq. 2 for systems with external potential, the black hole formation ef-

iciency was computed with Eq. 2.2. To compute these quantities, we use R_v (the external potential also had the same R_v); M_i ; N ; the mean stellar mass ($\overline{m_*} = M_i/N$); and r_* . The above-mentioned simulations extended over 10 Myr and resulted in the formation of very massive stars. They used the same assumption as in Reinoso et al. (2018) for the larger stellar radii, with the very massive stars ending up as a black hole. Neither Katz et al. (2015) nor Reinoso et al. (2020) provided a value for R_h , but they did provide the value for R_v . To approximate R_h , we used the relation typical for a Plummer profile, a virial radius of approximately $R_v \approx 1.7a$, and a half-mass radius of approximately $R_h \approx 1.3a$, where a is the Plummer radius, leading the following estimation of $R_h \approx 0.8R_v$. Vergara et al. (2021) investigated runaway collisions in both flat and rotating clusters using a Miyamoto-Nagai distribution (Miyamoto & Nagai 1975) with equal-mass stars. To compute the M_{crit} and ϵ_{BH} , we used the initial cluster mass and a half-mass radius of the radial plane, numbers of stars, and stellar mass as $m_* = M_i/N$, with a range of stellar radii, $r_* = 50, 100, 500, 1000 R_{\odot}$ (with the stellar radius used as a free parameter). The simulation time was 2 Myr and resulted in the formation of very massive stars. They also assumed these very massive stars will end as a black hole.

Panamarev et al. (2019) simulated the galactic center of the Milky Way, using one million stars, including a Kroupa (2001) IMF with masses ranging from 0.08 to 100 M_{\odot} . To assess the efficiency of black hole formation and the critical mass, we used an initial mass, half-mass radius, time ($\tau = 5.5$ Gyr), and the black hole mass taken from their Figure 7. In a different study, Vergara et al. (2023) investigated runaway collisions in NSCs, employing models with equal-mass stars distributed according to a Plummer distribution (Plummer 1911). To determine the critical mass and black hole formation efficiency, we considered the initial cluster mass, virial radii, stellar mass and radius, and the mass of very massive stars formed after $\tau = 10$ Myr. In Reinoso et al. (2018, 2020); Vergara et al. (2021), the authors assumed that very massive stars evolve enough time to form a black hole. We computed the half-mass radius using the same assumptions as Reinoso et al. (2020) and Katz et al. (2015). Besides Arca Sedda et al. (2023a,b,c) simulated star cluster using $(0.12, 0.3, 0.6, 1) \times 10^6$ stars, including a Kroupa (2001) IMF ranging from 0.08 to 150 M_{\odot} . These simulations also include primordial binaries up to 33% of the total number of stars. The simulations last around a few gigayears. We took the maximum black hole mass formed in the stellar system (see their Table 1).

Rizzuto et al. (2023) explored tidal disruption and capture runaway collisions in dense clusters, including post-Newtonian effects. The use of a Kroupa (2001) IMF, with a range between 0.08 to 2 M_{\odot} , the low-mass stars were chosen to avoid stellar evolution. They also include an initial black hole within the cluster with initial masses of 50, 300, and, 2000 M_{\odot} . Almost all the simulations run for times around 40 Myr. To compute the efficiency of black hole formation and the critical mass, we used an initial mass, the half-mass radius, the simulation time, and the black hole mass.

Appendix B: Cluster mass loss

The relation between the initial mass, M_i , and final mass, M_f , of stellar systems is not always well known. Simulations studying the formation of massive objects via collisions usually report the initial stellar mass of the system as well as the mass of the massive object that forms; sometimes, also additional information on the final stellar mass and the escapers is being reported. Observations, on the other hand, only report on the current state of a

stellar system. For the analysis in this paper, the relation between final and initial stellar mass can, however, be somewhat relevant and, therefore, this aspect is examined here in some detail.

As a first and very simple approximation, we could assume that the total mass in the system is conserved, namely, that there are no escapers and the mass exchange happens only between the stellar mass and the central massive object as a result of collisions. In this case, we have:

$$M_i = M_f + M_{\text{BH}}. \quad (\text{B.1})$$

In the case of the simulations, M_i and M_{BH} are known. The critical mass, M_{crit} , can be calculated from the initial conditions and M_f can be estimated from Eq. B.1. Employing this approximation, this allows us to plot M_f/M_i as a function of M_i/M_{crit} for the simulations, which we provide in the top panel of Fig. B.1. Under this assumption, we see clearly that for small ratios of $M_i/M_{\text{crit}} \lesssim 0.1$, $M_f/M_i \sim 1$, while it decreases for higher values of M_i/M_{crit} . This behavior should indeed be expected if the mass of the most massive object increases with M_i/M_{crit} .

We can test the approximation employed in Eq. B.1, at least for some simulations where both the initial and final stellar masses are available. For this purpose, we can employ the numerical simulations by Vergara et al. (2021, 2023) introduced above, for which we plot the relation both using the correct values from the simulation, and comparing with the result when instead using the approximation from Eq. B.1. In the bottom panel of Fig. B.1, we show that the results in both cases are qualitatively similar, however, when using the real data, the ratio M_f/M_i decreases somewhat more rapidly with increasing M_i/M_{crit} due to the escapers. This result also intuitively makes sense, as a higher ratio of M_i/M_{crit} implies a higher probability that interactions within the cluster have occurred, which can also lead to the ejection of stars from the system. From the data obtained here, we derive a polynomial fit to determine M_f/M_i as a function of M_i/M_{crit} . Our fit in the first case when employing Eq. B.1 is given as

$$\left(\frac{M_f}{M_i}\right)_{\text{noesc}} = a \log\left(\frac{M_i}{M_{\text{crit}}}\right)^2 + b \log\left(\frac{M_i}{M_{\text{crit}}}\right) + c, \quad (\text{B.2})$$

while when using the real data including escapers, we obtain

$$\left(\frac{M_f}{M_i}\right)_{\text{esc}} = d \log\left(\frac{M_i}{M_{\text{crit}}}\right)^2 + e \log\left(\frac{M_i}{M_{\text{crit}}}\right) + f. \quad (\text{B.3})$$

From the ratio between these two expressions, we can further derive a scale factor of

$$\alpha = (M_f/M_i)_{\text{noesc}} - (M_f/M_i)_{\text{esc}}, \quad (\text{B.4})$$

which can be employed as an approximate correction to estimate the effect of escapers when the information is not given. This procedure allows us to precisely take into account the mass exchange between mass in stars and the mass of the most massive object according to the simulation results, while the mass loss due to escapers is only estimated. The result of this estimate is given in Fig. B.2. We note that it shows a similar behavior as found in Fig. B.1, which, in principle, is natural as the basic trend is seen even when the mass loss due to escapers is not considered; this trend is then further enhanced when that possibility is taken into account.

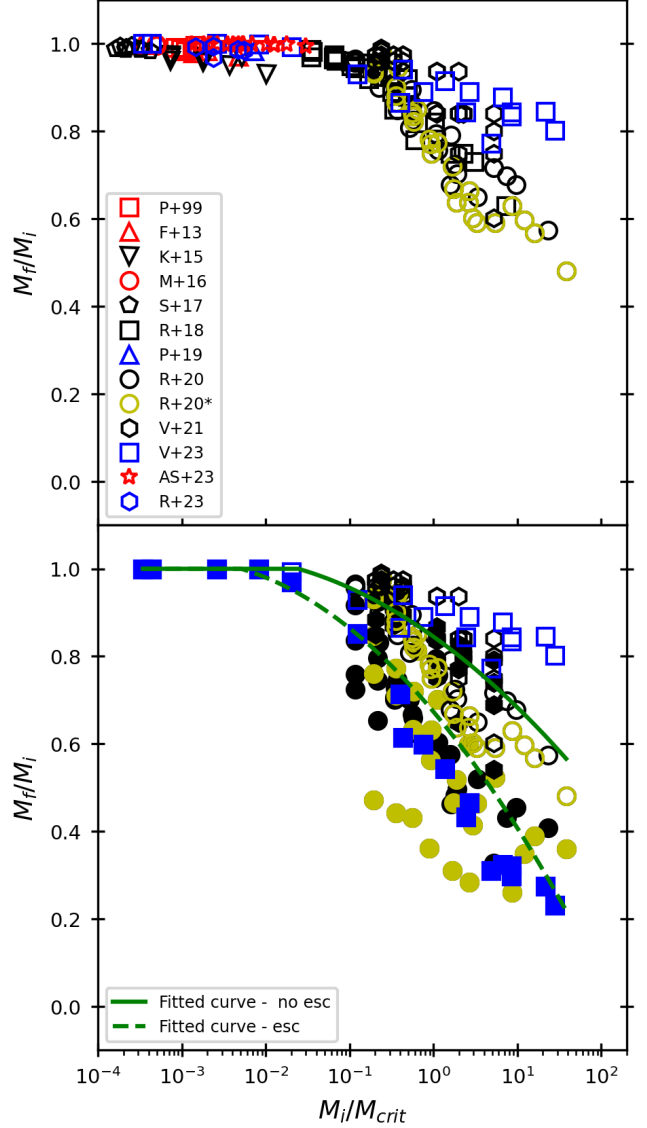


Fig. B.1. M_f/M_i as a function of M_i/M_{crit} , assuming that $M_i = M_f + M_{\text{BH}}$ for all simulations considered from Table 1 (top). M_f/M_i as a function of M_i/M_{crit} (bottom) using the simulations of Reinoso et al. (2020); Vergara et al. (2021, 2023). We show both the result as it would appear considering the approximation used in Eq. B.1 via the solid line and the result when we employ the initial and final stellar masses obtained from the simulation. In the second case the plot is qualitatively similar but with a steeper decrease due to the escapers. The figure also indicates our polynomial fits to the obtained relations.

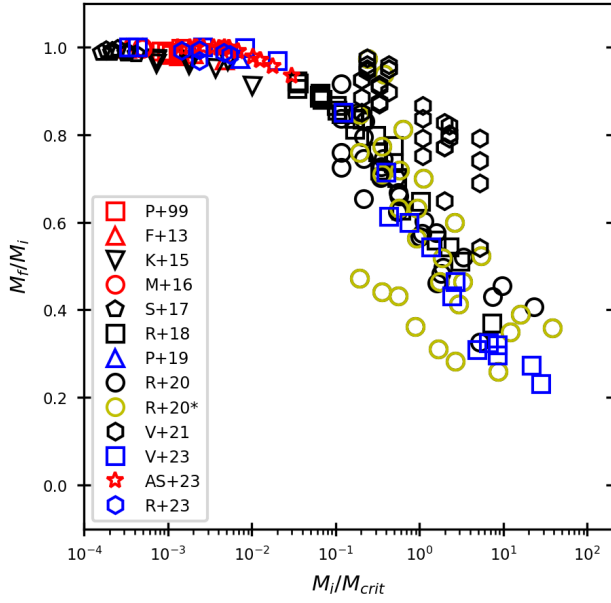


Fig. B.2. M_f/M_i as a function of M_i/M_{crit} in the simulations. Here M_f/M_i is calculated considering the stellar mass going into the most massive object and applying the correction factor α from Eq. B.4 to estimate the mass loss due to escapers.